



doi:10.1016/j.gca.2003.07.018

Early diagenesis of biogenic silica in the Amazon delta: Alteration, authigenic clay formation, and storage

PANAGIOTIS MICHALOPOULOS^{1,2*} and ROBERT C. ALLER[†]

Marine Sciences Research Center, State University of New York at Stony Brook, Stony Brook, New York 11794-5000, USA

(Received May 9, 2002; accepted in revised form July 3, 2003)

Abstract—Deltaic environments are commonly assumed to be relatively minor sites of biogenic silica burial because of the small quantities of opaline silica detected by most operational analytical techniques. Rapid conversion of biogenic silica into authigenic silicates is also often discounted as a significant control on oceanic silica budgets. A variety of evidence for extensive early diagenetic alteration of biogenic silica in rapidly accumulating Amazon delta sediments indicates that both of these general assumptions are unjustified. Apparent lack of significant biogenic silica storage in deltaic environments, particularly in the tropics, may be largely an artifact of operational definitions that do not include early diagenetic products of biogenic silica. Biogenic silica particles buried in suboxic Amazon delta deposits can be unaltered, partially dissolved, covered with aluminosilicate or metal-rich coatings, or completely reconstituted into authigenic K-Fe-rich aluminosilicate minerals. Pore water (K, Mg, F, Si) and solid-phase distributions, direct observations of particles, laboratory experiments, and depositional context indicate that authigenic clays form rapidly (<1 yr) in the seasonally reworked surface layer (~0.5–2 m) of the delta topset and are disseminated during sediment remobilization. Fe, Al-oxide rich debris derived from the tropical drainage basin is an abundant reactant, and thus the supply of biogenic silica is a major control on the amount of clay formed.

The mild 1% Na₂CO₃ alkaline leach procedure commonly used to estimate biogenic silica was modified to include an initial mild leach step with 0.1N HCl to remove metal oxide coatings and to activate poorly crystalline authigenic phases for alkaline dissolution. Well-crystallized clays are not significantly affected by this modification nor is bulk Amazon River bed sediment. The two-step procedure indicates that ~90% of the biogenic silica originally present in deposits is converted to clay or otherwise altered, raising the effective quantity of biogenic silica stored from ~33 to ~296 μmol Si g⁻¹ (~1.8% SiO₂). Biogenic Si stored in the delta increases away from the river mouth, across shelf and along the dispersal system where primary production is highest. The K/Si ratio of labile authigenic material is ~0.19 mol mol⁻¹, far higher than Amazon River suspended matter (~0.07 mol mol⁻¹). Diagenetic models indicate formation rates in the mobile sediment layer of ~2.8 μmol K g⁻¹ yr⁻¹ (~16 μmol Si g⁻¹ yr⁻¹). Inclusion of authigenic alteration products of biogenic silica in estimates of reactive Si burial increases the deltaic storage of riverine Si to ~22% of the Amazon River input. The rapid formation of aluminosilicates from biogenic SiO₂, seawater solutes, and remobilized Fe, Al-oxides represents a form of reverse weathering. Rapid reverse weathering reactions in tropical muds and deltaic deposits, the largest sediment depocenters on Earth, confirms the general importance of these processes in oceanic elemental cycles. Copyright © 2004 Elsevier Ltd

1. INTRODUCTION

It is widely assumed that biogenic silica reaching the seabed is subjected largely to simple dissolution, dehydration-recrystallization, or burial, and is not involved in complex mineral formation to any significant degree during early diagenesis. The operational analytical methods most commonly used to measure sedimentary biogenic Si are designed to be consistent with that assumption and do not explicitly target possible early diagenetic products. Consequently, estimates of the amounts of biogenic silica stored in marine sediments do not usually include the potential incorporation of biogenic silica into multiple diagenetic pools such as authigenic aluminosilicates (Ragueneau et al., 2000; Tréguer et al., 1995; Calvert, 1983; DeMaster, 2002). Relatively small changes in estimates of the quantity of biogenic Si, or its equivalent alteration products, stored in

high sedimentation rate environments such as deltas and continental rise deposits would have major impacts on models of global Si cycling (DeMaster, 2002).

It is well established that the surfaces of biogenic silica particles are often quickly coated and enriched in Fe and Al, dramatically affecting solubilities and dissolution behavior of Si in both the oceanic water column and sedimentary deposits (Lewin, 1961; Hurd, 1973; Katamani et al., 1988; Van Bennekom et al., 1989; Rickert et al., 2002). Al in particular can progressively permeate siliceous tests during initial deposition and burial (Van Bennekom et al., 1989; Dixit et al., 2001; Dixit and Van Cappellen, 2002). Close associations of biogenic silica with distinct authigenic aluminosilicate minerals have also been reported from a variety of depositional environments. For example, Hurd (1973) described the intimate intergrowth of authigenic Al, Si-phases with radiolarian tests in Pacific deep sea sediments, and proposed equilibration with such phases as one possible control on pore water Si(OH)₄ concentrations. Similar associations of authigenic clay and siliceous biogenic debris have been documented at numerous additional deep-sea sites (Sayles and Bischoff, 1973; Johnson, 1976; Heath and

* Author to whom correspondence should be addressed (pmichalo@nsmr.gr). Present address: Institute of Oceanography, National Center for Marine Research, Agios Kosmas, Ellinikon 166 04, Greece.

†(raller@notes.cc.sunysb.edu).

Dymond, 1977; Hein et al., 1979; Cole, 1985; Odin and Frohlich, 1988). Specific aluminosilicates have also been reported associated intimately with living diatoms in nearshore marine waters (van Bennekom and van der Gast, 1976), and obvious replacement of diatom frustules by poorly crystalline authigenic clay minerals occurs in saline lakes (Badaut and Risacher, 1982). Recent studies in the Southern Ocean have implicated control of pore-water silicate concentrations by authigenic aluminosilicate formation during early diagenesis (Van Cappellen and Qiu, 1997 a,b; Van Beusekom et al., 1997; Rabouille et al., 1997; King et al., 2000; Dixit et al., 2001). Bottom waters and pore waters in a wide range of nearshore high sedimentation rate deltaic and estuarine environments also typically show regular stoichiometric relationships between dissolved Al and Si, consistent with rapid, early diagenetic formation of authigenic aluminosilicates (Mackin and Aller, 1984, 1986, 1989; Mackin, 1986).

The involvement of biogenic silica in the formation of aluminosilicate phases has been discussed within the context of reverse weathering processes, *sensu* Mackenzie and Garrels (Michalopoulos and Aller, 1995; Mackenzie et al., 1981; Wollast, 1974; Wollast and Mackenzie, 1983; Mackenzie and Garrels, 1966). Reverse weathering reactions result in the formation of cation-rich aluminosilicate phases during early diagenesis and have been proposed as a significant component of oceanic elemental mass balances (Mackenzie and Garrels, 1966). The apparent lack of confirming evidence in initial searches for such reactions (e.g., Dasch, 1969; Russell, 1970) resulted in a tendency to discount their existence and to ignore many subsequent indications to the contrary (Savin and Epstein, 1970; Ristvet, 1978; Sayles, 1979; Mackenzie et al., 1981; Yeh and Eslinger, 1986; Mackin and Aller, 1989). Experimental and field studies of Amazon delta sediments in particular have demonstrated the existence of rapid, early diagenetic reverse weathering reactions in high sedimentation rate deposits, and indicated that in some metal oxide rich environments, such as tropical deltas, biogenic silica availability could be the limiting factor for the formation of authigenic aluminosilicate phases (Michalopoulos and Aller, 1995; Michalopoulos et al., 2000).

The present study reexamines sediment storage of biogenic silica in Amazon delta sediments and more fully evaluates the role of transformation of opaline Si into derivative minerals than done previously. We provide substantial additional quantitative and qualitative evidence from direct examinations of individual natural particles, sediment leach experiments, pore water compositions, local depositional context, and from large-scale spatial distributions, for the multiple diagenetic fates of biogenic silica in Amazon delta sediments. It is shown that a significant portion of riverine Si delivery is stored within the delta in a variety of sedimentary forms, including authigenic clays, although most dissolved Si probably transits the shelf. There is a consistent pattern of support from experimental and field measurements for rapid and substantial reverse weathering involving biogenic silica, reactive Al, Fe-oxides, and seawater solutes in tropical, shallow water muds and deltas such as the Amazon: classes of sedimentary deposits that dominate the present global sediment cycle (Bernier, 1982; Milliman and Syvitski, 1992; Ludwig et al., 1996).

2. BACKGROUND

2.1. Physical and Chemical Characteristics of the Amazon Continental Shelf

The Amazon River delivers $\sim 1.1\text{--}1.3 \times 10^9$ tons yr^{-1} of suspended sediment to its lower reaches (Mead et al., 1985), contributing up to $\sim 7\%$ of the global riverine input to the oceans. About 50–60% of this sediment is deposited on the continental shelf in the form of a subaqueous prograding delta, comprising characteristic topset, foreset, and bottomset clinoform strata (Nittrouer et al., 1986; Kuehl et al., 1986). Net sediment accumulation rates are highest in the foreset portion, where they reach values >60 cm/yr, and decrease both landward toward the topset region and seaward toward the bottomset (Kuehl et al., 1986; Dukat and Kuehl, 1995).

The physical regime on the shelf is extremely energetic, reflecting a combination of tides and tidal currents (up to ~ 6 knots), waves, river outflow, and the North Brazil current (Geyer et al., 1996). As a result, the top $\sim 1\text{--}2$ m of sediment in the topset is extensively physically reworked. Excess ^{210}Pb profiles in the upper 1–2 m of this region typically have constant activity with depth and unconformably overlie relict sediment having no excess activity (Kuehl et al., 1986, 1995). The underlying relict, consolidated deposits can be periodically exposed when the mobile sediment blanket is removed (Kuehl et al., 1986; Alexander et al., 1986; Allison et al., 2000). Within the mobile surface layer, sediment accumulates during multiple events of erosion/deposition. Seasonal sampling of benthic communities, sediment Fe oxidation states, pore water solutes, radionuclide distributions, diagenetic modeling, and water column inventories of Ra isotopes all indicate that the mobile surface layer is completely reworked annually or semiannually (Kuehl et al., 1995; Aller and Stupakoff, 1996; Aller and Todorov, 1997; Aller et al., 1996; Moore et al., 1996). The mass of sediment involved in this refluxing is huge, >18 Gt, and roughly equivalent to the mass of sediment delivered annually to the oceans by all rivers or to $\sim 15\text{--}30$ yr input by the Amazon River (Moore et al., 1996; Aller, 1998). The surface reworked layer is formed during multiple local erosion–deposition events, and is composed of layers of short-term net deposition separated by scour or hiatal surfaces (Kuehl et al., 1995). Overall net sediment accumulation and strata preservation proceeds as basal portions of the reworked layer escape subsequent erosional events, or as sediment is advected into less energetic regions of the delta (e.g., foreset) (Kuehl et al., 1996; Kineke and Sternberg, 1995; Cacchione et al., 1995).

2.2. Primary Productivity and Dissolved Silica Uptake in Amazon Shelf Waters

The main nutrient sources for Amazon shelf production are the Amazon River, upwelled offshore waters, recycled bottom water, and benthic fluxes (Ryther et al., 1997; Milliman and Boyle, 1975; DeMaster and Pope, 1996; DeMaster and Aller, 2001). The major source of dissolved Si to the outer shelf is the riverine input ($\sim 66\%$) with a smaller contribution from shoreward advection of offshore waters ($\sim 34\%$). Primary productivity is highest in a zone between the turbid nutrient-rich river plume waters inshore and the nutrient-poor blue surface waters in the offshore marine region. In this intermediate zone, pri-

primary productivity can be comparable to other highly productive regions such as the equatorial Pacific and the upwelling region off Peru ($>3 \text{ gC m}^{-2} \text{ d}^{-1}$; Smith and DeMaster, 1996). Other oceanographic parameters, such as the relative direction of winds and the river plume flow, can increase shelf water residence times and promote phytoplankton blooms.

A number of chemical and biologic parameters such as dissolved silica uptake, biogenic silica content of the suspended matter, and chlorophyll-*a* measurements, indicate that the dominant primary producers in these waters are diatoms (Milliman and Boyle, 1975; DeMaster et al., 1996). Nutrient budgets from water column measurements also show imbalances between the amount of dissolved silica removed from the water column and the standing crop of biogenic silica, indicating massive loss of particulate biogenic silica. Removal can be due to zooplankton grazing and other mechanisms of particle extraction, and can result in the non-steady-state deposition of biogenic silica in delta sediments or particle transport offshore or onshore (Milliman and Boyle, 1975; DeMaster et al., 1996).

2.3. Storage of Biogenic Silica in the Amazon Continental Shelf System

The role of the Amazon continental shelf as a sink of the riverine dissolved silica flux is considered minimal (DeMaster et al., 1983). Models indicate that the recycling of silica is very efficient, involving biologic uptake in surface waters and regeneration of dissolved silica in the water column and underlying sediments. The measure of overall recycling efficiency for silica, however, is based largely on the conclusion that only a small quantity of biogenic silica is stored in sediments. The earliest estimates of the biogenic silica content in Amazon delta deposits averaged 0.2% weight SiO_2 ($33 \mu\text{mol Si g}^{-1}$), which translates into storage of $\sim 4\%$ of the annual dissolved Si riverine input (DeMaster et al., 1983). Shiller (1996) utilized box models to infer that a far larger percentage of the riverine input, $\sim 15\text{--}30\%$ or greater, was likely stored on the shelf. The most recent published estimates balanced existing data on water column cycling and burial of biogenic Si, a portion of which were derived from early results of the present study, and calculated that $\sim 4\text{--}11\%$ of the river input are deposited in the delta (DeMaster and Aller, 2001). These calculations have considerable uncertainty but generally imply that the Amazon shelf is a relatively poor trap for silica.

3. MATERIAL AND METHODS

3.1. Sample Collection

Sediment cores were collected for biogeochemical studies during the AmasSeds project at a range of sites across the delta topset and upper foreset zone. Kasten cores ($\sim 2\text{--}3 \text{ m}$) and box cores ($\leq 0.5 \text{ m}$) were obtained seasonally at three stations established along each of two primary transects termed River Mouth Transect (RMT) and Open Shelf Transect (OST) (Fig. 1; see Aller et al., 1996). Seasonal sampling took place in August 1989 (period of falling river flow), February 1990 (rising flow), May 1990 (high flow), and October 1991 (low flow). In October 1991, piston cores up to 8 m length were retrieved at two sites along OST (PC 4204 [OST-2] and PC 4213 [OST-3]), from one station along RMT (PC 4228 [RMT-2]), and from a

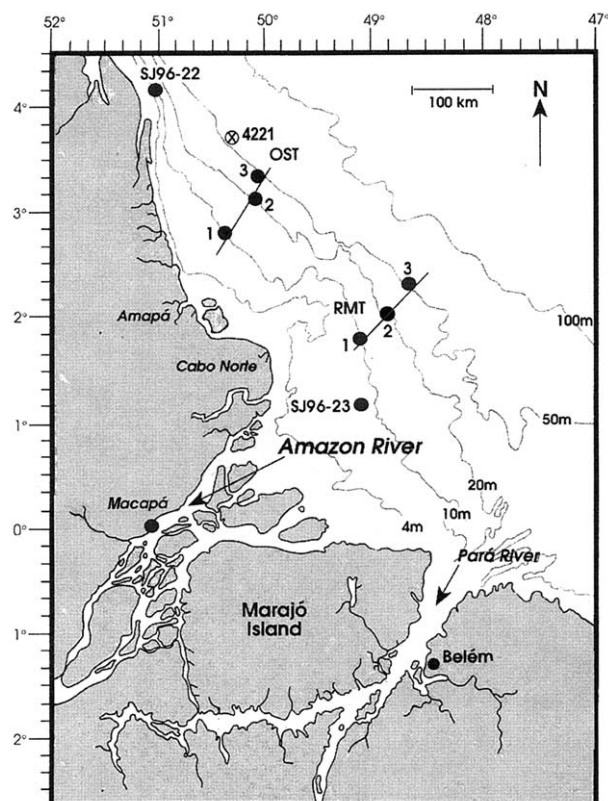


Fig. 1. Study region and location of sampling stations. Piston core station 4221 is located in an area of exposed relict material and referred to as the Relict Gas Site.

fourth station located in exposed, methanogenic relict deposits to the north of OST (PC 4221; Relict Gas Site) (Fig. 1). Additional kasten core samples were obtained during March 1996 at station SJ96-22; located in $\sim 7 \text{ m}$ of water 10 km off the coast of Amapá, Brazil ($4^\circ 10.64564\text{N}$, $51^\circ 01.99896\text{W}$; R/V Seward Johnson, Cruise 95-104). Station SJ96-22 ("Station 22") lies in the initiation region for the migrating mud waves that characterize the Guianas coast line downdrift of the Amazon delta (Allison et al., 2000).

After core retrieval, sediment was subscored, sectioned into $\leq 10\text{-cm}$ intervals, packed under N_2 (glove bag) into 250-mL polypropylene bottles, and pore-waters were separated using centrifugation (see Aller et al., 1996, for additional details). After removal and filtration of pore water, the resulting sediment plug was frozen ($\sim -20^\circ\text{C}$). Sediment was subsequently thawed for solid-phase analyses, and sampled where no signs of oxidation were obvious (away from the bottle walls). At SJ96-22, the kasten core was also carefully subsampled within specific intervals ($<1 \text{ cm}$) that exhibited easily recognizable black, Fe-sulfide rich layers. In the case of these dissected intervals, samples were not centrifuged but were placed directly into plastic scintillation vials and frozen.

Amazon River bed surface sediment was obtained from the north channel off the town of Macapá, Brazil ($\sim 0.01\text{N}$, $51^\circ 0.01 \text{ W}$; October 1996). A station located in the river mouth, SJ96-23 ($1^\circ 09.87\text{N}$, $49^\circ 05.36\text{W}$) was also sampled using a gravity core. Sediment in both cases was stored frozen.

3.2. Mineral Separations

In addition to direct microscopic examination of unmanipulated material, two different grain separation and concentration methods were utilized: a) heavy-liquid density fractionation, and b) wet-sieving grain size separation.

3.2.1. Heavy-liquid Separation

Wet centrifuged sediment (~10 g) was transferred to a centrifuge tube, washed three times with distilled-deionized (DI) water, centrifuged and the supernatant decanted. Washed sediment was resuspended in DI water and centrifuged to separate the >5- μm fraction from the fine-grained fraction which remained in suspension. The fine-grained suspended fraction was discarded. The >5- μm fraction was freeze-dried and transferred into a glass centrifuge tube. A heavy liquid (tetrabromoethane, TBE, $\rho = 2.96 \text{ g cm}^{-3}$) was introduced and after shaking, the heavy fraction was separated using centrifugation (~750 rpm, 10 min). The heavy fraction was filtered and washed repeatedly with acetone until TBE was not detectable. The resulting separate was examined with a binocular microscope and grains were carefully handpicked.

3.2.2. Wet Sieving Separation

Frozen sediment was thawed, rinsed briefly with distilled-deionized water, centrifuged and the supernatant decanted. After three rinse treatments, the centrifuged sediment plug was resuspended in DI water and wet sieved through a stack of 125-63-38 μm metal sieves. Storage, microscopic observation and handpicking of the separated grains were done while the grains were immersed in DI water to ensure particle hydration and to avoid agglutination during drying. Diatom particle counts were obtained from size fractions with a stereomicroscope and from unfractionated samples with an inverted microscope. Operational Si leaching experiments, as described subsequently, were also performed on the fine sand (63–125 μm) fraction.

3.3. Scanning Electron Microscopy (SEM), Elemental Mapping, and Transmission Electron Microscopy (TEM)

General morphologic observations of particles were carried out with a JEOL scanning electron microscope (SEM). A SuperJEOL SEM was also used for qualitative EDS chemical analyses. A JEOL 200CX TEM equipped with an EDS system was used for detailed morphologic and chemical studies. (See Michalopoulos et al., 2000 for additional details on sample preparation and TEM results).

3.4. Pore-water Analyses

Acidified subsamples of pore water (pH ~ 2, 0.1N HCl) were analyzed for K, Mg, and Si (precision of ~ 3%, 2%, 2% respectively). Potassium was analyzed using flame emission or atomic absorption spectroscopy, magnesium using flame atomic absorption (La suppressor), and Si with the molybdate-blue method (Strickland and Parsons, 1968). Cl^- was analyzed

on unacidified samples using a Radiometer CMT10 titrator (1% precision).

3.5. Biogenic Silica Leaches

Estimation of biogenic silica and early diagenetic alteration products are critical for quantification of mass fluxes and silica burial. The most generally accepted operational method for biogenic silica analyses utilizes the time-dependent release pattern of dissolved Si from sediment exposed to ~1% Na_2CO_3 (~0.1 mol/L) at 85°C over ~ 2–10 h (DeMaster, 1991; Conley, 1998). A variety of stronger alkaline leaches have also been used along with inferred corrections (Al release) for aluminosilicate contributions (Eggemann et al., 1980). In most studies, sediment is usually oven dried and ground or crushed before extraction, and may also be pretreated with H_2O_2 and acid (Mortlock and Froelich, 1989). A hyperbolic relationship between dissolved Si concentration and time is often observed (e.g., $\text{Si} \propto \tanh(t)$; $\text{Si} \propto \text{arcsinh}(t)$), and is interpreted as resulting from a combination of rapidly dissolving biogenic Si and more slowly dissolving crystalline silicates. The tangent to the concentration vs. time function, usually averaged over a time interval such as 2–5 h, is extrapolated to time zero. The extrapolated concentration (y intercept) is used to estimate the mass of the most reactive silica phases responsible for the initial rapid release of Si on sediment exposure to alkaline solution. This mild alkaline leach method typically recovers ~80% of fresh diatoms added as standard additions to marine sediments, and far lower percentages of less soluble forms of silica such as sponge spicules or robust diatoms (e.g., Eggemann et al., 1980; DeMaster, 1991; Gehlen and Van Rapphorst, 1993). Use of the time series release pattern, as opposed to a single concentration measurement at a specific time, is particularly important when biogenic SiO_2 is <3% of bulk sediment (Mortlock and Froelich, 1989).

As shown in the results section, when examined in detail, Si release from Amazon delta sediments exposed only to 0.1M Na_2CO_3 does not usually follow the commonly reported asymptotic release pattern (Fig. 10). Instead, the rate of Si release continues to increase after a few hours (e.g., $\text{Si} \propto \sinh(t)$). Acceleration of rates presumably reflects progressive increase in the availability of reactive sites. The presence of even minor Fe, Al, or thin mineral coatings can inhibit biogenic silica dissolution rates by more than an order of magnitude in mild alkaline solutions, making such particles quite comparable in relative dissolution behavior to crystalline clays (Lewin, 1961; Rickert et al., 2002; Dixit and Van Cappellen, 2002). It is clear from numerous previous studies that the presence of coatings (metal oxides, aluminosilicates) on biogenic silica will prevent accurate analysis by mild alkaline leach techniques. Amazon delta sediments are characterized by suboxic conditions and extensive Fe and Mn cycling (Aller et al., 1986, 1996), making it a virtual certainty that all biogenic Si in Amazon shelf deposits is reacted with remobilized metals and metal oxides, and thus compromising the a priori kinetic assumptions in standard analytical techniques. In addition, direct observations (see "Results") demonstrate other major modes of surface protection or occlusion of biogenic silica by authigenic minerals.

Exposure of biogenic silica, both planktonic and sedimentary, to mineral acids is known to remove metal oxide coatings

and to enhance subsequent dissolution rates of silica in either natural waters or alkaline leach solutions (Lewin, 1961; Hurd, 1973; Mortlock and Froelich, 1989; Rickert et al., 2002). Most acid treatments utilized for activation of biogenic Si and removal of coatings in previous studies are harsh, however, and designed for essentially pure opaline SiO₂ samples. Strong acid treatments will clearly attack detrital silicates and are not appropriate for complex lithogenic mixtures.

Leaches with mild acids such as 0.1N HCl have been successfully utilized to dissolve poorly crystalline metal oxides and authigenic silicates in both relatively pure silicate precipitation experiments or complex natural mixtures (Mackin, 1987; Gehlen and Van Rapphorst, 1993). Poorly crystalline authigenic clays in diatom frustules can apparently even dissolve in distilled water within 24 h (Badaut and Risacher, 1982). Weak HCl solutions leach Si from detrital clays, but less so than do mild alkaline solutions such as 0.1M Na₂CO₃ (Eggimann et al., 1980; Mackin and Swider, 1987; see also subsequent "Results"). For reasons that we will further justify in the "Results" section, to remove metal coatings, poorly crystalline authigenic minerals, and to activate biogenic silica surfaces for subsequent alkaline dissolution, we chose to utilize a mild acid treatment, ~0.1N HCl, at room temperature before leaching in alkaline solution. We found that if sediment were exposed to this two-step mild acid–mild alkaline extraction procedure, rather than a single alkaline extraction, the Si release patterns became regular, repeatable, and consistent with a wide range of other qualitative and quantitative observations. Because all operational techniques can be controversial, however, we give conversion factors between various standard analytical methods for reactive silica pools in Amazon delta sediments.

To extract reactive Si, frozen sediment samples were thawed and replicate ~25–35 mg wet sediment subsamples immediately leached with 25 mL of 0.1N HCl in 50 mL polyethylene centrifuge tubes at room temperature (T ~ 22°C). Samples used for leaching were never dried or ground. Tubes were either constantly or periodically shaken (no discernable differences found). Subsamples of sediment, dried at 60°C, were utilized to obtain wet/dry weight ratios. Two durations of HCl pretreatments were used (1h and 18 h) in different sets of samples. HCl leaches were analyzed for dissolved Si and K. After centrifugation and removal of the HCl, sediment was rinsed briefly and centrifuged twice with several milliliters of distilled water to remove residual acid. Remaining sediment was subsequently leached for 7–8 h with 25 mL of 1% Na₂CO₃ (~0.1 mol/L) at 85°C and serially sampled. To compare different operational pools, selected samples were also analyzed using the alkaline leach for biogenic Si without an acid pretreatment. For consistency with previous estimates of biogenic silica reported by DeMaster et al. (1983), we used results in this latter case from only the first 5 h of reaction. These various operational pools are defined as: Si-HCl (mild acid leachable), BSi (mild alkaline leachable, no acid pretreatment), Si-Alk (mild alkaline leachable after acid pretreatment), and ΣSi [total reactive Si released by acid and subsequent alkaline treatments = (Si-HCl) + (Si-Alk)]. Where appropriate, these terms are modified to indicate specific reaction times. Analogous operational pools are defined for K⁺.

4. RESULTS

4.1. Particle Morphology and Alteration

4.1.1. Heavy Liquid Separates

Microscopic examination of heavy mineral samples revealed distinctive diatom frustules and discoid grains ranging in size from 20–300 μm. The occurrence of both classes of particles in the heavy separates resulted from framboidal pyrite-filled centers ($\rho_{\text{pyrite}} \sim 5.00 \text{ g cm}^{-3}$). In some cases, diatom cells had readily recognizable frustule microarchitecture, whereas in others, extensive frustule destruction and filling of frustule aureoles with precipitates were obvious (Fig. 2). The most common type of heavy particle were discoid composite aggregates, consisting of a central core of framboidal pyrite coated by a layer of aluminosilicate material (Fig. 3). Individual framboids have diameters that range from ~4–15 μm. The size and shape of these whole composite grains are indistinguishable from centric diatom frustules found in overlying water and in the sediments (Fig. 3B). Polished sections and SEM observations of individual discoid grains demonstrated that the outer aluminosilicate layer can contain siliceous domains (Fig. 3D).

4.1.2. Wet Sieved Separates

The microscopic examination of the wet-sieved grain separates also revealed the presence of three main diatom-derived particle populations: i) visually unaltered whole diatom frustules, ii) corroded diatom frustules, and iii) completely altered diatoms. In these cases, grains could be either filled with pyrite or not (i.e., low or high density). The completely altered particles retain the original shapes of diatoms but do not exhibit a well-preserved microarchitecture. Other biogenic siliceous particles, such as radiolarians, are also altered and coated with aluminosilicate precipitates (Fig. 4).

Detailed electron microscope observations and microprobe analyses in conjunction with the study of the pyrite-filled particles from heavy mineral separates allowed further division of the completely altered diatoms into two subclasses: a) altered diatom cells consisting of authigenic aluminosilicates with no evidence of detrital clay, and b) diatom pseudomorph composite grains with an aluminosilicate outer layer made of detrital matrix material cemented by authigenic aluminosilicate. The cell remnants lacking detrital clay have a fragile, membranous appearance and were found whole or separated into components (i.e., valves, girdle). Whole, altered frustules can also be separated into components during manipulation. TEM examination of these altered frustules revealed relics of the original microarchitecture (Michalopoulos et al., 2000). The authigenic aluminosilicate material that replaces the siliceous frustule consists of a dominant smectitic phase, which contains variable amounts of Fe and K, and a secondary cation-poor aluminosilicate phase (Michalopoulos et al., 2000).

4.2. SEM/Elemental Mapping/TEM

SEM observations of well-preserved diatoms or radiolarians revealed the presence of obvious surface coatings (Figs. 2 and 4) as well as internal alteration of biogenic particles. In some cases, frustules appear to have sections that are altered in close proximity to unaltered areas (Fig. 2). EDS/elemental mapping

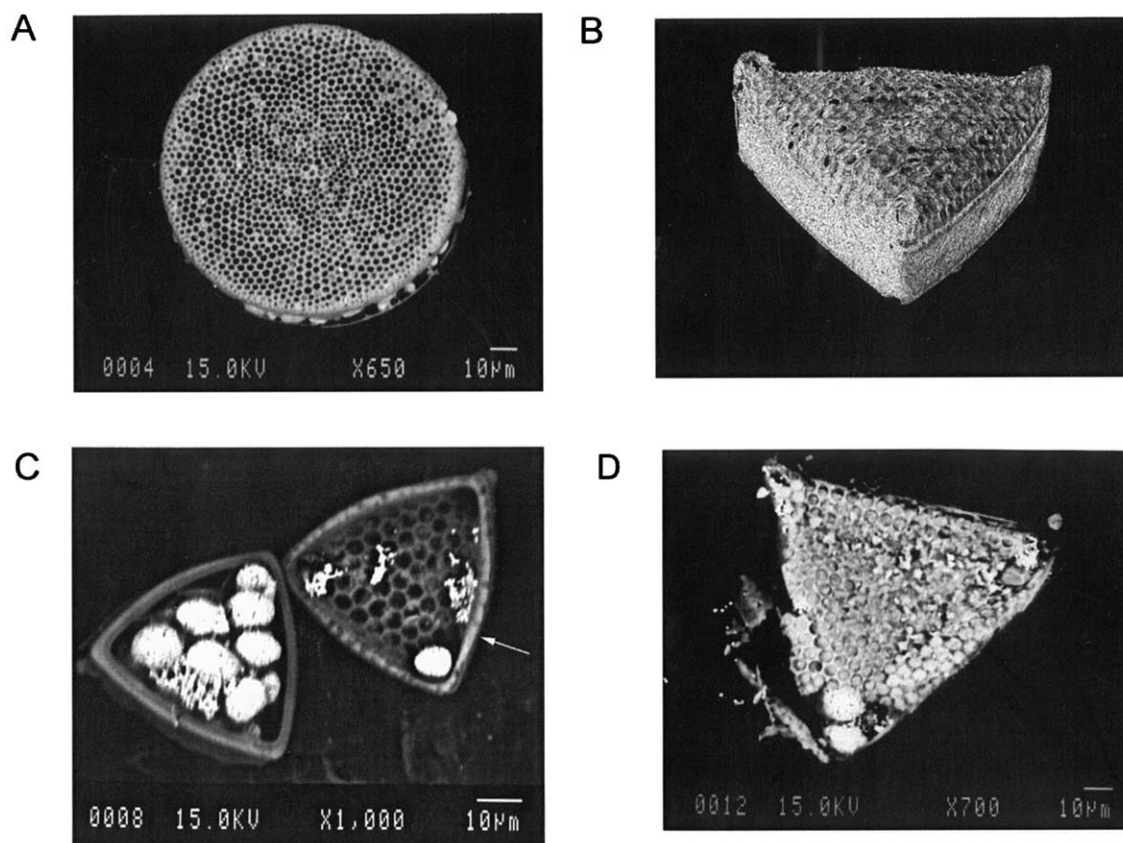


Fig. 2. Representative SEM images illustrating range of preservation modes of distinct diatom cells. (A) Discoid diatom cell from OST-2 (393–403 cm). Parts of the frustule aureoles are covered by aluminosilicate coatings. (B) Triagonal diatom, *Triceratium favus*, with nearly continuous authigenic aluminosilicate and metal-rich coating. (C) Valves of triagonal diatom opened to reveal internal framboidal pyrite fill. Parts of the frustule exhibit enrichments in K, Al, and Fe (arrow) whereas the remainder is unaltered. (D) Diatom in advanced stages of alteration and initial fragmentation. The microarchitecture is recognizable but extensively altered. Aureoles are filled with aluminosilicate precipitate, and the cell lumen is occupied by framboidal pyrite (from OST-2, 425–435 cm).

shows a range of compositions of the authigenic aluminosilicate material associated with frustules. Pyrite-filled diatom pseudomorphs can have aluminosilicate layers that are virtually Fe-free. In other cases where minimal amounts of pyrite are present, the aluminosilicate material invariably contains abundant Fe (Fig. 5). Detailed TEM observations of reconstituted diatom frustules showed that the diatom frustules can be replaced by a variety of crystal types, including euhedral cation-rich aluminosilicate crystallites, individual flakes, or crystal bundles (Michalopoulos et al., 2000). Lattice-fringe measurements show that most of these flakes have basal spacings of 10.2–11 Å, and consist of Si, Al, K, Mg, and Fe (Fig. 6A,B). Euhedral crystallites that formed in frustules during anoxic incubations of cultured diatoms in the laboratory are also composed largely of Si, Al, K, Fe, and Mg (Fig. 6C). The average compositions of Amazon delta sediments, authigenic clay crystals replacing buried diatoms, and clay crystals formed during incubation experiments with cultured diatoms are shown in Table 1. The K/Si mole ratio tends to be higher in the marine authigenic clays (0.11–0.13) compared to average Amazon delta (0.07) and Amazon River (0.05–0.07) suspended sediment.

4.3. Diatom Abundance/Degree of Alteration

The abundance of diatom-shaped particles from sediment subsamples was estimated as a function of depth in the kasten core recovered from Station 22 (SJ96-22; off Amapá). ^{210}Pb activity distributions and diagenetic properties demonstrated that this site had a suboxic, mobile surface layer of sediment ~80 cm thick overlying relict methanogenic deposits (Fig. 7A; Allison et al., 2000; Zhu et al., 2002). As noted earlier, this two-zone sedimentation and diagenetic structure is typical of Amazon shelf sediments. Total diatom counts were obtained using microscopic examinations (lower particle size resolution ~10 μm) of bulk sediment samples. Diatom point counts of particles >38 μm were estimated with a stereomicroscope. The diatom size fraction between 10 and 38 μm was calculated by subtracting the >38 μm counts (stereomicroscope) from total counts made using an inverted microscope. Total diatom counts in the top ~80 cm are between 6×10^4 and $14 \times 10^4 \text{ g}^{-1}$ of dry sediment (Fig. 7B). Small diatom particles (>38 diameter >10 μm) have equal or greater abundance than large >38 μm diatom particles over most of the mobile layer. Counts drop precipitously below ~80 cm at the base of the mobile zone to

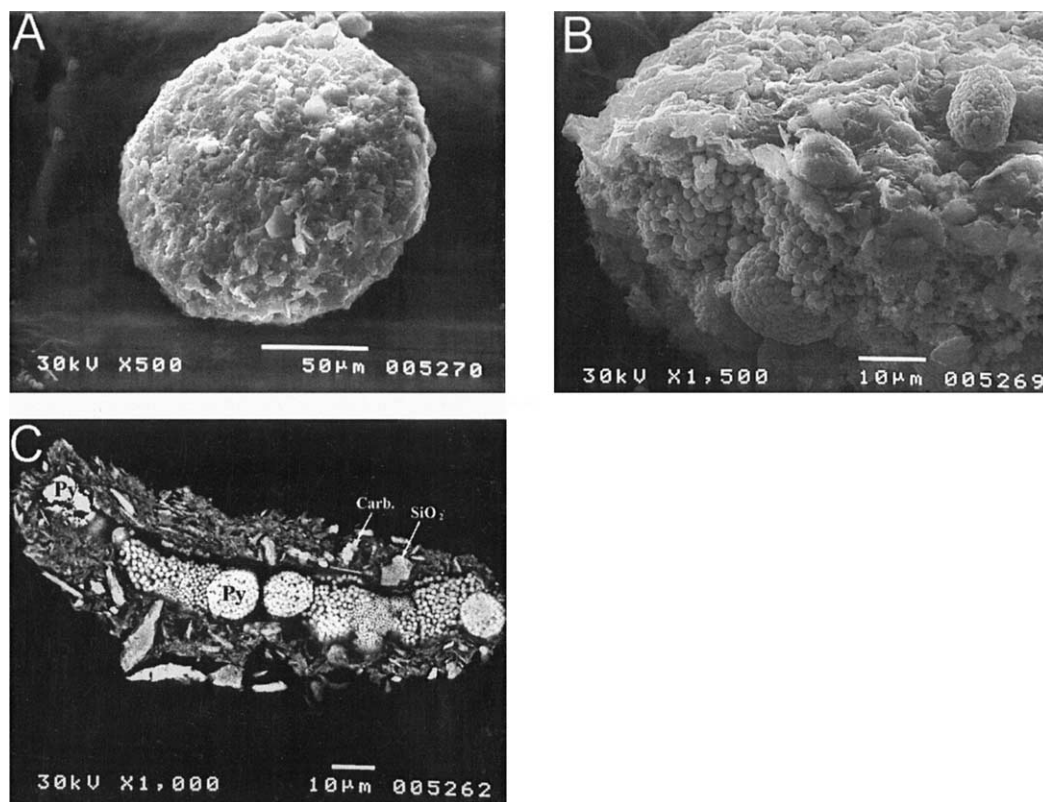


Fig. 3. Representative SEM images of pyrite-filled composite clay aggregates. (A) Whole centric diatom pseudomorph (OST-2; 216–226 cm) (scale bar = 50 μm). (Compare size–shape to Fig. 2A). (B) Broken diatom pseudomorph showing exposed interior framboidal pyrite presumed comparable in source to Figure 2C (OST-2, 216–226 cm). (C) Complete cross section of a pseudomorph composite (OST-2 425–435 cm). Py denotes the framboidal pyrite infill of the residual cell chamber. The external layer consists of residual domains of SiO_2 frustule and detrital matrix components cemented by authigenic precipitates. (Backscatter image; scale bar = 10 μm).

a range of $\sim 10\text{--}7000\text{ g}^{-1}$, and the smaller size class is virtually absent in this underlying material. Diatoms are significantly higher in subsamples obtained from FeS-rich black layers when present (e.g., at 132.5 cm) than in adjacent sediments.

Diatom particles from the $>38\text{ }\mu\text{m}$ size fraction were further subdivided into two classes based on appearance, fresh or altered. For this division, fresh diatoms retained visual evidence of frustule microarchitecture while altered diatoms did not, and were corroded or broken. The abundance ratio of visually altered to total diatom particles in the $>38\text{ }\mu\text{m}$ size fraction was used as an alteration index (A.I.). Diatoms from the upper $\sim 80\text{ cm}$ of the core have similar degrees of alteration (A.I. ~ 0.1). There is a clear transition in the degree of alteration at the base of the mobile zone ($\sim 80\text{ cm}$) below which the proportion of altered diatoms increases fivefold to A.I. ~ 0.5 to 1. In several deep FeS layers the alteration index is ~ 1 .

4.4. Pore Water Analyses

Pore water solute profiles reflect balances between diagenetic reactions and seasonal sediment dynamics in the upper $\sim 1\text{--}2\text{ m}$. As demonstrated by examples from topset station OST-2, extensive exchange of pore water can occur seasonally during reworking of the mobile zone (Fig. 8A,B). Constituents, such as Si(OH)_4 , produced in deposits are depleted after major

periods of seafloor mobilization (e.g., rising to high river flow). Constituents such as K^+ , consumed in deposits, tend to be replenished from overlying water. Correspondingly, during relatively stable periods (e.g., falling to low river flow), reaction products build up (Si(OH)_4) and reactants are relatively depleted (K^+) (see additional examples in Aller et al., 1996). Si(OH)_4 concentrations in the surface mobile zones grade into higher values in underlying relict deposits (Fig. 8C). Distributions of Si(OH)_4 , K^+ , and Mg^{++} over greater depth intervals ($\sim 7\text{ m}$; Fig. 9) demonstrate that gradients are maintained over many meters within consolidated sediments. Gradients decrease with depth, however, reflecting decreasing reaction rates below the mobile zone. Dissolved silica concentrations reach values up to $\sim 380\text{ }\mu\text{M}$ at OST-2. Asymptotic Si values well below opaline silica solubility ($\sim 1.2\text{ mM}$) are typical of Amazon delta sediments ($\sim 50\text{--}500\text{ }\mu\text{M}$; Mackin and Aller, 1986; Michalopoulos and Aller, 1995), and indicate that reactions other than simple amorphous silica equilibria are controlling concentrations (Hurd, 1973; Mackin, 1986). Dissolved K^+ , Mg^{++} , and F^- uptake with depth are also general characteristics of Amazon delta deposits (Aller et al., 1986; Rude and Aller 1994).

Pore water Cl^- at the Macapá riverbed site was $<1\text{ mM}$ (detection limit) and 56 mM at the river mouth station SJ96-23.

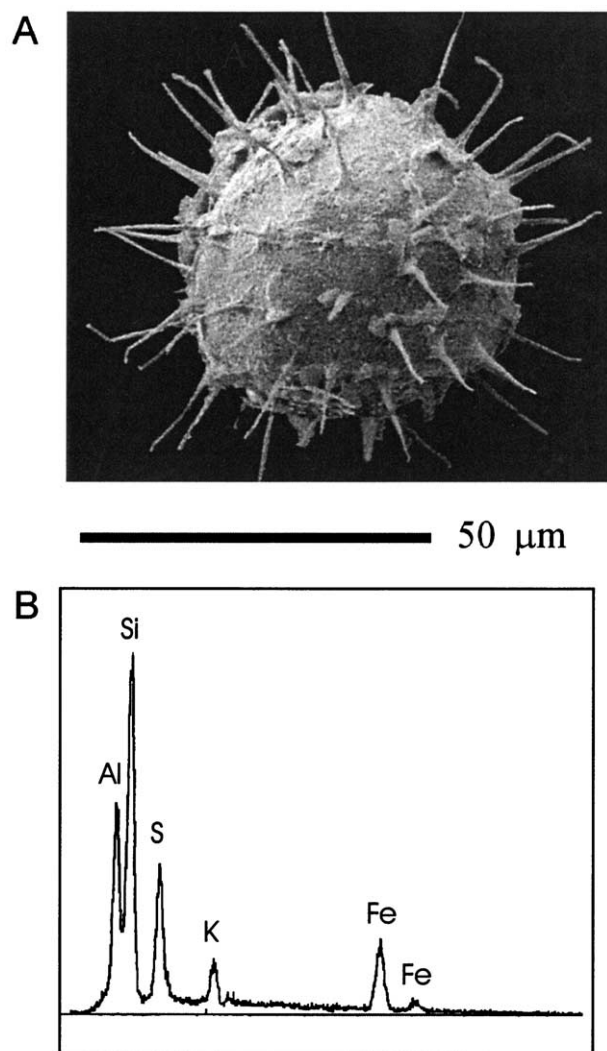


Fig. 4. Non-diatom siliceous debris can also be morphologically well-preserved but highly altered. (A) Whole radiolarian extensively coated by authigenic clay and filled with pyrite. (B) EDS spectra of surface coating (center of (A)) demonstrating the K, Fe-rich composition typical of Amazon delta authigenic clays (S from pyrite).

RMT-1 pore waters ranged from ~ 350 – 450 mM and OST-1 from ~ 260 – 350 mM, while all remaining delta topset sites were >500 mM (up to 570 mM offshore). SJ96-22 off Amapá had pore water $\text{Cl}^- \sim 320$ – 525 mM over the upper 2.5 m.

4.5. Biogenic and Reactive Sedimentary Silica

4.5.1. Operational Extractions of Reactive Silica

Analysis of >50 Amazon delta topset sediment samples demonstrated that the release rate of dissolved Si from samples treated only with 1% Na_2CO_3 usually increases with reaction time, producing concave-upward concentration vs. time functions in $>80\%$ of samples (Fig. 10A). These patterns demonstrate that the primary assumptions of the mild alkaline leach method regarding dissolution kinetics are not generally valid for these deposits. Previous estimates of Amazon delta biogenic

silica contents utilized extrapolations from the first 5 h of leaching where the nonlinearity is poorly expressed (DeMaster et al., 1983). After mild 0.1N HCl pretreatment, either 1 or 18 h, it was found that the time-series Si release patterns with subsequent 1% Na_2CO_3 leach were largely linear after ~ 1 – 2 h, allowing reliable estimation of a reactive Si pool by linear extrapolation (Fig. 10B). Samples that gave the highest evidence for accelerated rates (nonlinearity) with time of alkaline leach (no pretreatment) were not always completely linearized by 1 h 0.1N HCl pretreatment, whereas almost all samples were linear after 18 h pretreatment. After the mild acid preleach, the size of the labile Si pool estimated from alkaline leaches (Si-Alk) was substantially increased in delta sediments (Fig. 10).

Examples of the absolute and relative sizes of the operational Si pools are shown in Figure 11 for the Amazon River bed station at Macapá and for the average of six samples taken from the upper 6 m at OST-3 (3–13, 38–48, 80–90, 514–524, 545–555, 577–587 cm intervals, multiple replicates). Because riverbed sediments were sandy mud, both the bulk and <63 μm size fractions (wet sieved) were analyzed, the latter to better reflect suspended load. The river and delta sediments show major differences in both the absolute and relative magnitude of operational Si pools. Total reactive Si ($\Sigma\text{Si} = \text{Si-HCl} + \text{Si-Alk}$) is far higher at the delta (~ 412 $\mu\text{mol g}^{-1}$) compared to riverbed site (~ 56 – 102 $\mu\text{mol g}^{-1}$). BSi represents a substantial portion of ΣSi in the riverbed ($\text{BSi}/\Sigma\text{Si} = 0.50$ – 0.66), compared to OST-3 ($\text{BSi}/\Sigma\text{Si} \sim 0.08$). In addition, Si released by alkaline leach with or without an acid preleach is relatively similar in the river material ($\text{BSi}/\text{Si-Alk} \sim 0.67$) compared to OST-3 ($\text{BSi}/\text{Si-Alk} \sim 0.13$). These differences in the relative magnitude of operational pools are maintained at all sites across the delta despite changes in ΣSi (Table 2). The average reactive pool ratios at delta sites seaward of rivermouth station SJ-23 are $\text{Si-HCl}/\Sigma\text{Si} \sim 0.35$, $\text{BSi}/\Sigma\text{Si} \sim 0.41$, $\text{Si-Alk}/\Sigma\text{Si} \sim 0.59$, and $\text{BSi}/\text{Si-Alk} \sim 0.34$. Acid pretreatment therefore has a substantially larger effect on Si release patterns from delta compared to river sediment and increases estimates of reactive Si by a factor of ~ 5 – $10\times$ (BSi vs. ΣSi).

For comparison, operational Si pools were also examined in standard reference clays, kaolinite (API #9), montmorillonite (API # 27), and illite (Ward Scientific, Rochester shale). Kaolinite, montmorillonite, and illite (10 Å clay) compose $\sim 36\%$, 27% , and 28% of Amazon River clays respectively (Gibbs, 1977). Offshore deposits in the OST-3 region are largely clay (average grain size of ~ 10 phi) composed of $\sim 25 \pm 7\%$ kaolinite, $\sim 33 \pm 17\%$ smectite, $\sim 4 \pm 2.6\%$ illite-smectite, $\sim 36 \pm 13\%$ illite, and trace chlorite (Kuehl et al., 1986, 1995; Dukat and Kuehl, 1995). In contrast to the handling of wet sediment samples, the standard clays (dry) were gently ground before extraction. Total reactive Si in standard clays ranged from $\Sigma\text{Si} \sim 20$ – 140 $\mu\text{mol g}^{-1}$ (Table 2). Clay standards released smaller quantities of Si after acid leach than did delta samples, comparable to or less than Amazon river bed deposits (Table 2). The relative importance of operational Si pools was very different in standard clays than delta deposits and was similar to the riverbed and river mouth samples, averaging: $\text{Si-HCl}/\Sigma\text{Si} \sim 0.35$, $\text{BSi}/\Sigma\text{Si} \sim 0.76$, $\text{Si-Alk}/\Sigma\text{Si} \sim 0.65$, and $\text{BSi}/\text{Si-Alk} \sim 1.1$. Thus, acid pretreatment has a relatively small effect on the subsequent release of Si from

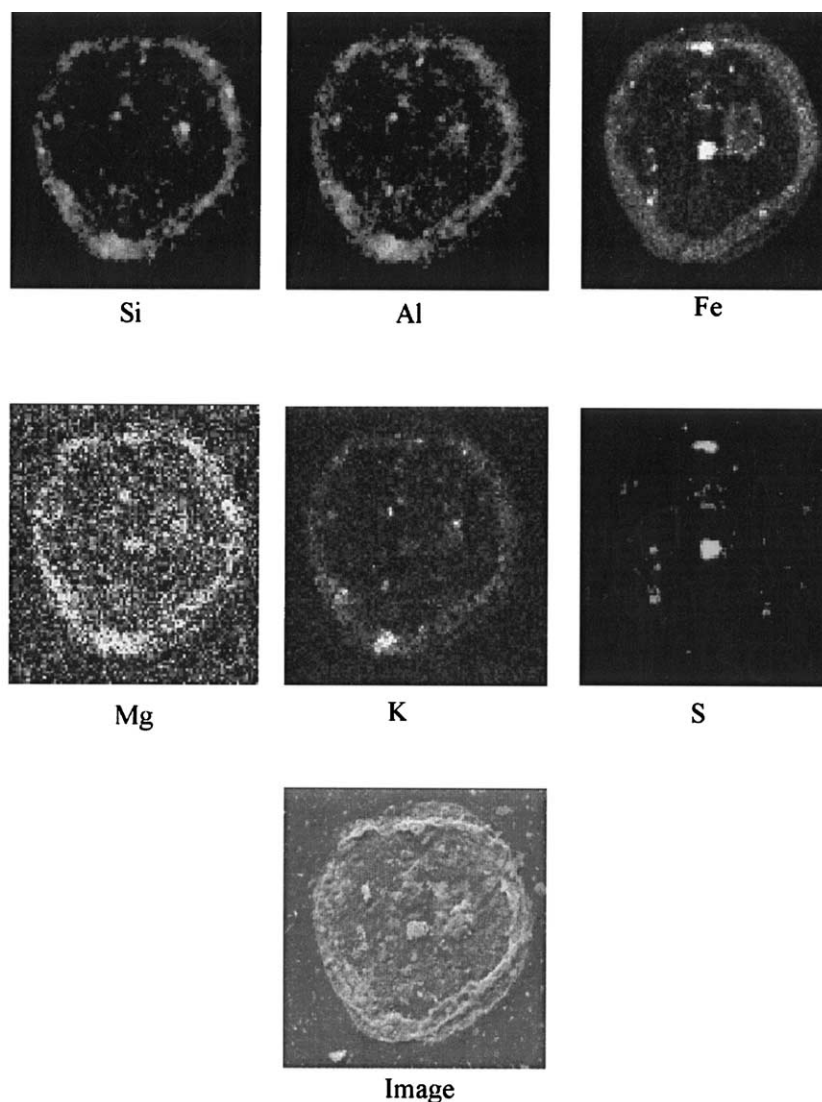


Fig. 5. Elemental map (EDS) of a frustule remnant (Station 22, depth = 95 cm). The “membranous” authigenic aluminosilicate that has replaced the original siliceous frustule contains K, Fe, and Mg. In this case only a small amount of central pyrite is present. In cases where pyrite-fill is abundant, altered clays are often relatively Fe-poor.

standard clays by mild alkaline solution. As in the case of Amazon riverbed samples, the Si released from standard clays by mild alkaline treatment alone (BSi) is comparable to the Si released by alkaline leach after acid pretreatment (Si-Alk). Previous studies have reported magnitudes of Si release from standard clays during the BSi procedure or during leaching with 0.1N HCl (Si-HCl) similar to those found in the present study (e.g., Eggimann et al., 1980; Mackin and Swider, 1987).

A portion of the Si released by 0.1N HCl (Si-HCl) may be derived from Fe, Mn, Al-oxides. The quantities of Fe extracted by 0.1N HCl from delta station OST-3 sediment are $\sim 19 \pm 1 \mu\text{mol Fe g}^{-1}$ and $\sim 78 \pm 12 \mu\text{mol Fe g}^{-1}$ in 1 h and 18 h respectively. For comparison, ~ 7 and $44 \mu\text{mol Fe g}^{-1}$ are extracted by 1 mol/L NH_2OH -0.175 mol/L Na-Citrate, and 76 and $227 \mu\text{mol Fe g}^{-1}$ are extracted by 0.2 mol/L Na-oxalate in 1 h and 18 h respectively (a standard 4 h Na-Oxalate leach extracts $\sim 172 \mu\text{mol Fe g}^{-1}$). These latter two solutions are

often used as operational extractants for highly reactive Fe-oxides in marine sediments (Robbins et al., 1984; Canfield, 1989). Typical ranges of Si/Fe mole ratios reported from similar operational extractions of soils are ~ 0.1 – 0.3 (Parfitt and Childs, 1988). Total bulk analyses of completely altered ferrous laterites give maximum Si/Fe ~ 0.7 – 0.9 (Tardy, 1997). The soil extractions thus suggest that $<20 \mu\text{mol Si g}^{-1}$ might be released by 0.1N HCl from Fe, Mn, Al-oxides at delta sites and even less at coarser grained stations proximal to the river mouth. Coastal French Guiana deposits derived from the Amazon River release $\sim 10 \mu\text{mol Si g}^{-1}$ during extraction by 0.2 mol/L Na-oxalate (Panzeca and Aller, unpublished). These estimates are far lower than the measured release of Si by 0.1N HCl from Amazon delta sediments (Table 2).

To more directly check the efficiency of extraction of altered diatom material by the different operational treatments, we handpicked highly altered but recognizable diatom particles

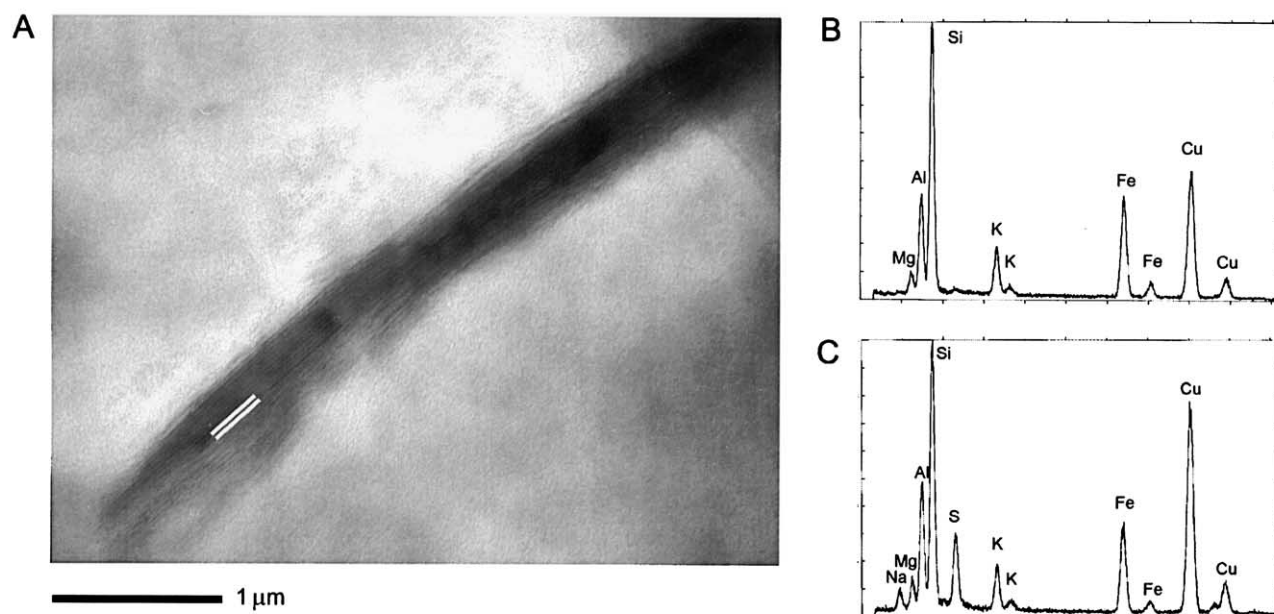


Fig. 6. (A) Lattice fringe image of an authigenic crystal that has replaced a siliceous diatom frustule (Station SJ96-22 depth = 200 cm). In this case, the measured basal spacing (white lines) is approximately 10.2 Å. (B) TEM/EDS spectrum of the authigenic crystal shown in (A) demonstrating dominance of Si, Al, K, Fe, and Mg. (C) TEM/EDS spectrum of an euhedral clay crystallite that replaced the cultured *Coscinodiscus* sp. incubated anoxically in Amazon mud for 23 months (see Michalopoulos et al., 2000). The composition is comparable to the in situ alteration product (B). S is due to FeS from cell decomposition. Cu signal is from the sample holder.

from sediment samples and subjected them to extraction. These altered diatoms released $\text{BSi} = 101 \mu\text{mol Si g}^{-1}$ compared to $\text{Si-Alk} = 184 \mu\text{mol Si g}^{-1}$. Microscopic observations of leached material revealed that highly altered frustules visually survived both leach methods and could maintain their morphology, particularly in the standard BSi procedure. The modified operational leach with the acid-pretreatment step is more effi-

cient in dissolving both the converted buried biogenic silica and the authigenic aluminosilicate phases replacing frustules. However, even with the two-step modified operational leach, converted frustules are not completely dissolved. In fact, only a very small portion of totally altered diatoms is dissolved either with the alkaline leach alone or with the acid-alkaline leach combination. The microleach experiment indicates that the

Table 1. Elemental ratios in Amazon River, Delta, and authigenic particles.

	Al/Si (mole/mole)			K/Si (mole/mole)			Fe/Si (mole/mole)		
	Mean	Range	SE	Mean	Range	SE	Mean	Range	SE
Amazon River suspended particulate matter	0.46	0.45 ^a –0.48 ^b	0.02	0.058	0.048 ^a –0.068 ^b	0.01	0.12	0.10 ^a –0.14 ^b	0.02
Average Amazon delta sediment (<63 mm) ^c	0.60	0.22–0.94	0.029	0.07	0.01–0.17	0.0078	0.13	0.02–0.28	0.012
Average authigenic clay replacing natural diatom frustules ^d	0.69	0.47–0.89	0.043	0.11	0.00–0.25	0.026	0.10	0.02–0.25	0.023
Average authigenic clay formed during diatom incubation experiments ^e	0.41	0.05–0.78	0.087	0.13	0.00–0.20	0.0267	0.17	0.03–0.42	0.043

^a Data from Martin and Meybeck (1979). Number of analyses $n = 1$.

^b Data from Sholkovitz and Price (1980). Number of analyses $n = 2$.

^c Chemical analyses obtained with an electron microprobe equipped with WDS. Number of analyses $n = 26$.

^d Semiquantitative chemical analyses obtained with a TEM equipped with an EDS. Number of analyses $n = 12$.

^e Semiquantitative chemical analyses obtained with a TEM equipped with an EDS. Number of analyses $n = 9$.

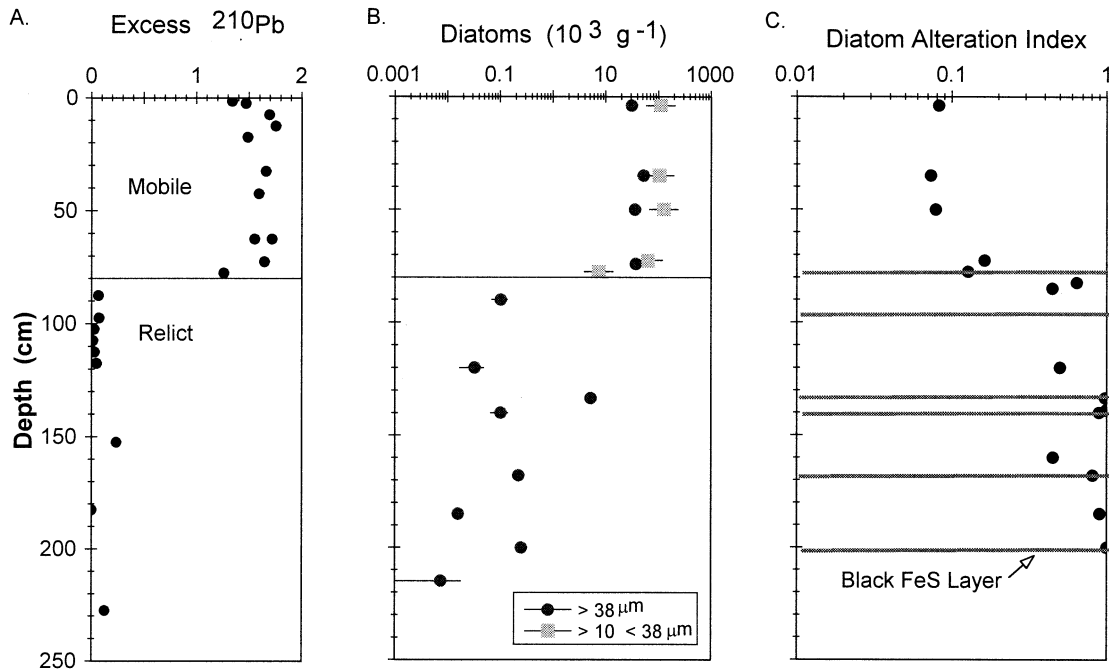


Fig. 7. (A) Excess ^{210}Pb distribution at station SJ96-22 located in proto-mudwave deposits off Amapá (adapted from Allison et al., 2000). The two zone pattern of a surface mobile zone (in this case ~ 80 cm) overlying consolidated relict deposits is typical of Amazon shelf deposits. (B) Both small and large diatoms are present in the mobile zone. Whole recognizable diatom frustules are rare in the underlying relict zone, and small cells are virtually absent. (C) About 10% of large diatom cells in the surface mobile layer are obviously altered (A.I. ~ 0.1). The percentage increases to $\sim 100\%$ in relict deposits and greater fragmentation is obvious (A.I. ~ 1).

operational leaches used in this study do not dissolve all the reconstituted biogenic silica present in Amazon deltaic sediments and are probably conservative estimates of biogenic silica and diagenetic alteration products (Table 3).

We conclude that for Amazon delta sediments the best estimate for total reactive sedimentary Si at present is the sum of the 18 h 0.1N HCl leach and Si-Alk. These mild procedures in tandem provide a reasonable balance between the need to

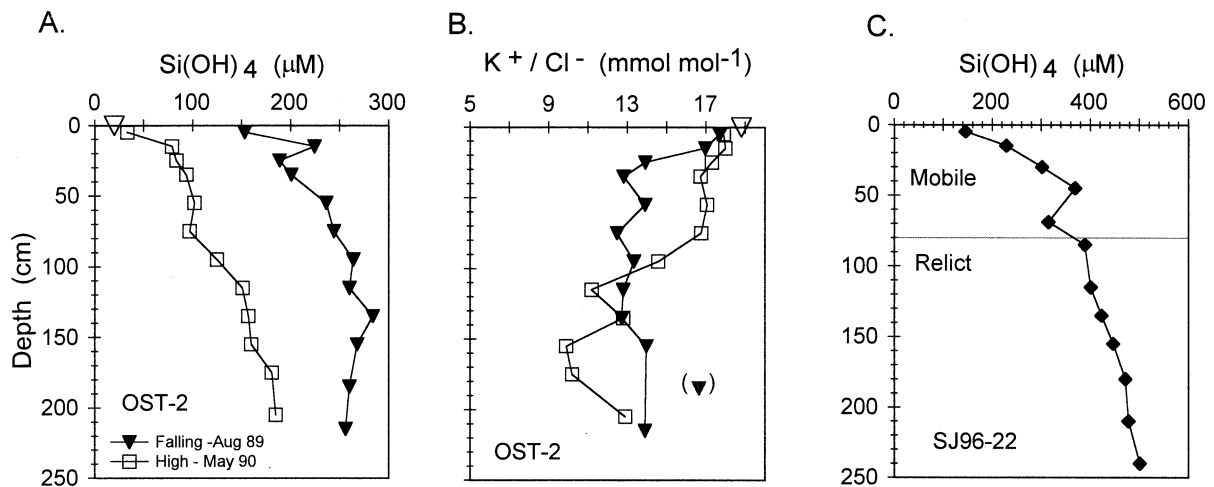


Fig. 8. (A) Example of seasonal variation in pore water $\text{Si}(\text{OH})_4$ at topset station OST-2. Low concentrations correspond to the period after recent remobilization of upper ~ 2 m. High concentrations follow the period of relative stability of sediment and ingrowth of reaction products. (B) Seasonal pore water K^+ concentration corresponding to (A). Normalization to Cl^- demonstrates conclusively that the pattern is diagenetic. Relatively high K^+ is observed in upper ~ 1 m following the period of pore water exchange. (Point in parentheses is interpreted as analytical error). (C) $\text{Si}(\text{OH})_4$ pore water profile at station SJ96-22 demonstrating gradation for mobile surface zone concentrations into underlying relict material in upper ~ 2 –3 m.

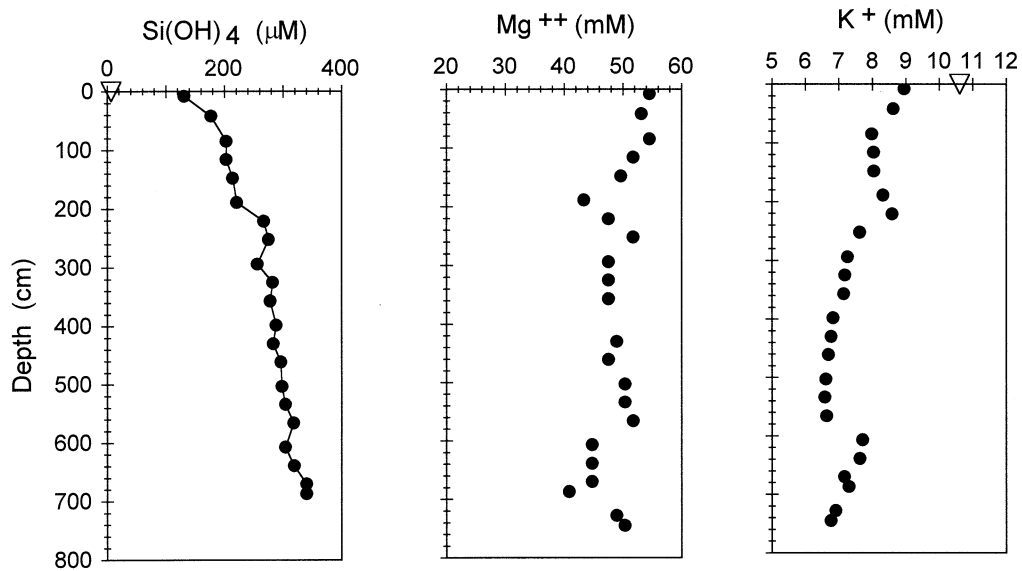


Fig. 9. Reactive solute concentration gradients decrease below the surface mobile zone (~ 2 m) but are discernable in this case to depths up to at least ~ 7 m at OST-2 (piston core). Uptake of K^+ and Mg^{++} and the relatively low asymptotic concentration of $Si(OH)_4$ are consistent with authigenic clay formation. (Overlying water values indicated by open triangles).

extract biogenic silica and altered products of biogenic silica, while largely discriminating against detrital material. Although the method does not extract all alteration products of biogenic Si and additional forms of Si such as Fe, Al-oxide associations are partially included, it is clearly a better approximation than mild alkaline leaches alone, and interferences are relatively minor compared to the overall analytical signal. The modification allows consistent and repeatable analytical treatment of data (e.g., linear extrapolation), and can be readily compared with operational methods available in the literature utilized for extraction of authigenic precipitates, oxides, and standard clays. As will be shown, environmentally consistent patterns and stoichiometric flux estimates are also obtained from this assumption.

To allow possible interconversion of analytical quantities, the concentrations of Si-Alk measured after either of the two HCl pretreatment times (1 h, 18 h) were compared directly on >60 sediment samples from the delta topset and off Amapá (SJ96-22). This comparison of the two acid pretreatments showed that the estimates of Si-Alk after 18 h HCl pretreatment were $\sim 1.3\times$ the value of Si-Alk after a 1-h HCl pretreatment (Si-Alk [1 h HCl] ~ 0.75 Si-Alk [18 h HCl]). The ratio of Si-HCl released after 18 h vs. 1 h is ~ 3.4 . The magnitude of BSi extracted by the alkaline leach alone (no pretreatment) from our delta core samples was comparable ($\sim 55 \pm 20 \mu\text{mol Si g}^{-1}$) to those reported by DeMaster et al. (1983) (average $33 \mu\text{mol Si g}^{-1}$). It should be further noted, however, that our BSi

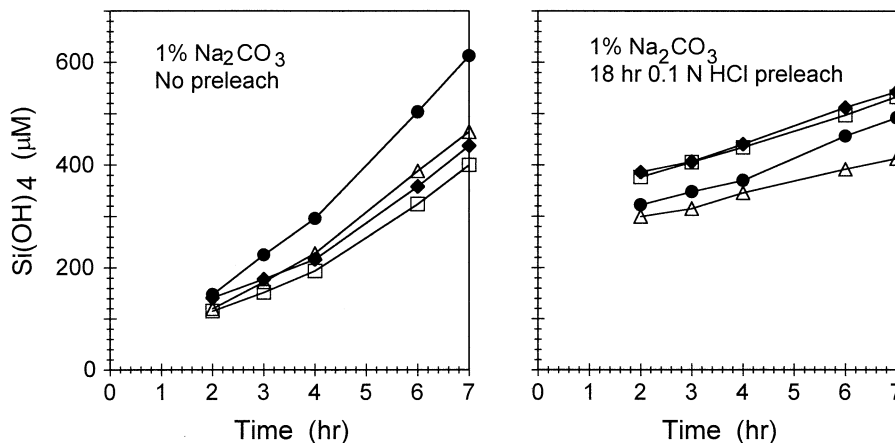


Fig. 10. (A) Representative examples of Si release patterns during extraction with $0.1 \text{ mol/L Na}_2\text{CO}_3$ at 85°C . Rate of Si release increases with time after ~ 4 – 5 h in $\sim 80\%$ of samples examined from both surface and relict deposits. (B) Examples of Si release during extraction by $0.1 \text{ mol/L Na}_2\text{CO}_3$ after a mild acid pretreatment (18 h, 0.1N HCl). Release is essentially a linear function of time after ~ 1 – 2 h.

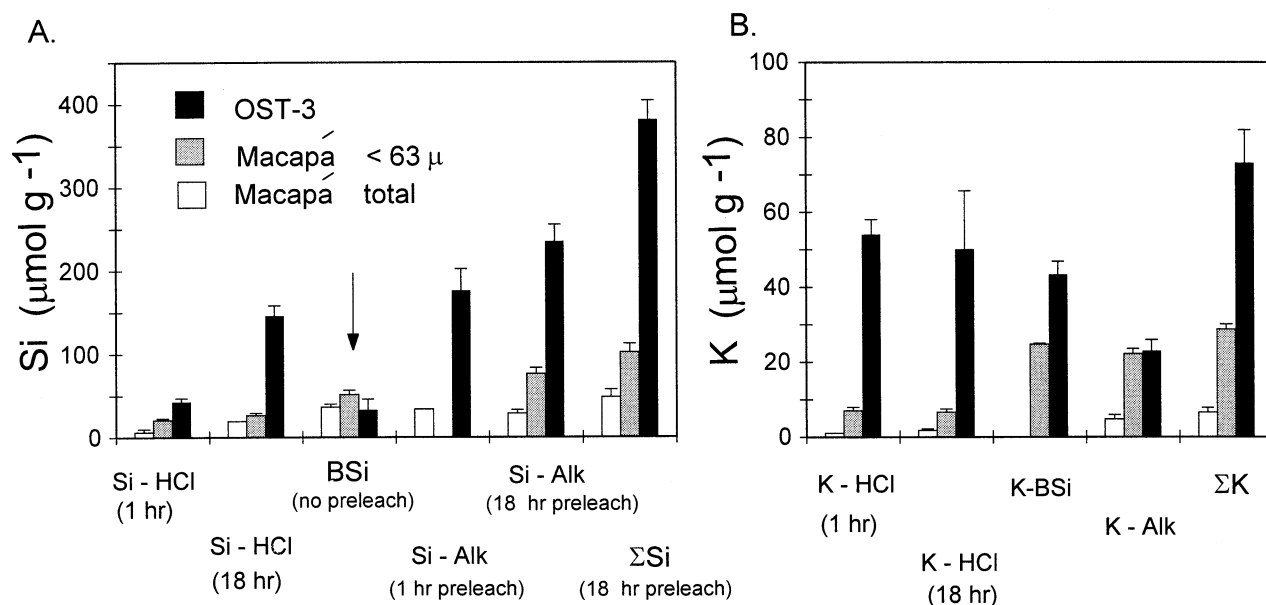


Fig. 11. (A) Comparison of operational reactive Si pools from Macapá (Amazon River: riverbed bulk and $<63 \mu$ fraction) and station OST-3 (upper 5 m), the most distal delta site sampled. BSi indicates the reactive Si released by the traditional 0.1 mol/L Na_2CO_3 (85°C) leach alone. Mild acid pretreatment results in dramatic increases in measured reactive Si pools in delta sediments but not in the river deposits. Even a brief acid leach (1 h) activates the alkaline leachable component in delta sediments but not in riverbed material or clay standards. (B) The corresponding reactive K pools demonstrate large increases of reactive K and dominance of the acid leachable pool (incongruent K, Si dissolution) at OST-3 relative to river sediment.

measurements were made directly on undried, unground samples as extrapolated intercept values (5 h), whereas the previously reported BSi values were made on dried, ground samples and corrected for an inferred analytical grinding effect. The grinding effect correction (derived from the mean of 5 samples extracted twice with 1% Na_2CO_3) reduced the calculated BSi concentrations by roughly half (DeMaster et al., 1983).

4.5.2. Stoichiometry and Magnitude of K and Si Release

As in the case of Si, a well-defined reactive K pool was present; however, the time-dependent patterns of K^+ released from sediment and the relative importance of acid and alkaline extractions differed from Si (Fig. 11). Approximately 98% of the K extracted from delta sediment by 0.1N HCl was released in 1 h. For example, at station SJ96-22 off Amapá, the ratio of K-HCl (18 h)/K-HCl (1 h) was 1.026 ± 0.0016 throughout the upper ~ 2.5 m ($n = 15$). The ratio averaged 1.1 ± 0.1 in bulk or $<63 \mu\text{m}$ fractions of Amazon riverbed sediment (Table 2). Similarly for alkaline treatment, virtually all K extracted over 7–8 h by 0.1M Na_2CO_3 in delta samples leached previously with 0.1N HCl (18 h) was released in the first 2 h ($\geq 90\%$) with little increase thereafter. If the mild alkaline leach is carried out without any prior acid treatment (as per BSi analysis), essentially all K-BSi is also released in the first 2 h of the mild alkaline leach. In contrast to reactive Si, the majority portion of the total reactive K ($\Sigma\text{K} = \text{K-HCl} + \text{K-Alk}$) in delta sediment was released by acid, with average $\text{K-HCl}/\Sigma\text{K} \sim 0.70$ (Table 2). K-BSi corresponds to about half of the total ΣK in delta deposits seaward of SJ-23, averaging $\text{K-BSi}/\Sigma\text{K} \sim 0.54 \pm 0.14$ (Table 2). Thus, there is a labile K pool released predominantly

by acid (70%) but with a significant proportion released only during alkaline dissolution ($\text{K-Alk}/\Sigma\text{K} \sim 0.3$). Approximately 21% of the ΣK pool reacts with either mild acid or alkaline solution ($(\text{K-BSi} - \text{K-Alk})/\Sigma\text{K}$). In sharp contrast to delta deposits, the K-HCl pool is far smaller in Amazon riverbed sediments and represents a relatively minor proportion of ΣK ($\text{K-HCl}/\Sigma\text{K} \sim 0.25 \pm 0.03$) (Table 2).

Reactive K pools in standard clays were distinctive to respective mineralogies and differed substantially from Amazon delta deposits both in magnitude and the relative importance of different pools (Table 2). ΣK was $200\text{--}500\times$ lower in kaolinite and $4\text{--}9\times$ lower in montmorillonite standards than in delta deposits. In the case of montmorillonite, the K-HCl pool accounted for $>90\%$ of release. In contrast to delta sediments, these standard clays had a readily detectable time-dependent release of K during alkaline treatment. During mild alkaline treatment (post 18 h HCl), kaolinite released $\sim 36\%$ K in the first 2 h ($1.2 \mu\text{mol K g}^{-1}$ total in 7 h) and montmorillonite $\sim 54\%$ ($2.2 \mu\text{mol K g}^{-1}$ total in 7 h).

The magnitude of K release from illite shale was significant but release patterns differed substantially from either Amazon River or delta sediment (Table 2). K was released from illite continuously with time by both mild acid and mild alkaline leaches. The ratio of K-HCl (18 h)/K-HCl (1 h), for example, was ~ 1.8 . In contrast to Amazon delta deposits, illite K-HCl $<$ K-Alk, $\text{K-Alk}/\Sigma\text{K}$ is relatively high (0.60 vs. 0.30 for average delta), and acid pretreatment had a substantial effect on the quantity of alkaline leachable K (K-BSi $<$ K-Alk) (Table 2).

Reactive K and Si pools are highly coherent in surficial delta deposits (0–15 cm) and increase progressively away from the

Table 2. Reactive Si and K contents of standard clays, Amazon River, and Delta sediments^a

Sample	Si-HCl (1 h)	Si-HCl (18 h)	BSi	Si-Alk (post HCl 18 h)	ΣSi	Si-HCl/ΣSi	BSi/ΣSi	Si-Alk/ΣSi
Kaolinite	1.6 ± 0.3	4.2 ± 0.8	25 ± 7	16 ± 5	20.2 ± 5.1	0.21	1.24	0.79
Montmorillonite	11 ± 0.5	49 ± 2	98 ± 1.3	91 ± 17	140 ± 17	0.35	0.70	0.65
Illite	30 ± 6	27.4 ± 1	18 ± 3	27 ± 2	54.4 ± 2.2	0.50	0.33	0.50
Amazon River SPM ^b			160					
Macapá (channel)	6.4 ± 3.6	20 ± 0.1	37 ± 3	29 ± 6	56 ± 9	0.39	0.66	0.61
Macapá (<63 μ)	21 ± 2	26 ± 3	51 ± 5	76 ± 8	102 ± 9	0.25	0.50	0.75
SJ-23 (river mouth)		61 ± 3	73.2 ± 3.5	89 ± 6	150 ± 6.7	0.41	0.49	0.59
RMT-1		87 ± 20	45 ± 38	98 ± 34	185 ± 39	0.47	0.24	0.53
RMT-2		98 ± 22	40 ± 19	121 ± 32	219 ± 39	0.45	0.18	0.55
RMT-3		111 ± 20	55 ± 19	161 ± 26	272 ± 33	0.41	0.20	0.59
OST-1		119 ± 17	90 ± 10	178 ± 30	297 ± 35	0.40	0.30	0.60
OST-2		110 ± 11	72 ± 46	170 ± 21	280 ± 24	0.39	0.26	0.61
OST-3	43 ± 4	146 ± 12	33 ± 13	235 ± 20	412 ± 31	0.39	0.08	0.61
Amapá (SJ-22)	36.4 ± 0.5	103 ± 2.7	51 ± 7	204 ± 13	309 ± 13	0.33	0.17	0.66

	K-HCl (1 h)	K-HCl (18 h)	K-BSi	K-Alk (post HCl 18 h)	ΣK	K-HCl/ΣK	K-BSi/ΣK	K-Alk/ΣK
Kaolinite	0.0	0.07 ± 0.09		0.10 ± 0.06	0.17 ± 0.1	0.41		0.59
Montmorillonite	8.2 ± 0.05	9.0 ± 0.3		0.64 ± 0.04	9.6 ± 0.3	0.93		0.07
Illite	15.6 ± 0.1	27.4 ± 0.06	24.3	41	68.4 ± 14	0.40	0.36	0.60
Macapá	1 ± 0.02	1.3 ± 0.3		4.8 ± 1.1	6.6 ± 1.2	0.27		0.73
Macapá (<63 μ)	7.1 ± 0.9	6.7 ± 0.8	24.7 ± 0.3	22 ± 1.4	28.7 ± 1.6	0.23	0.86	0.77
SJ-23 (river mouth)		15.4 ± 0.4		13.7 ± 0.8	29.1 ± 0.9	0.53		0.47
RMT-1		25.7 ± 3.9	13.1 ± 0.3	10 ± 2.0	35.7 ± 4.4	0.72	0.37	0.28
RMT-2		27.8 ± 10.1	22.6 ± 0.2	11.9 ± 2.7	39.8 ± 10.5	0.70	0.57	0.30
RMT-3		27.9 ± 9.0	22.4 ± 0.9	12 ± 3.4	39.9 ± 9.6	0.70	0.56	0.30
OST-1		40.2 ± 6.0	33.4 ± 2.4	22.7 ± 2.3	62.9 ± 6.4	0.64	0.53	0.36
OST-2		50.1 ± 8.3	29.6 ± 0.5	23 ± 2.9	73.1 ± 8.8	0.69	0.41	0.31
OST-3		50 ± 11.6	43.3 ± 3.5	33.8 ± 2.3	84 ± 4.8	0.60	0.59	0.40
Amapá (SJ-22)	32 ± 2.1	33 ± 4.6	39.6 ± 0.8	16.2 ± 3.5	49.2 ± 5.8	0.67	0.81	0.33

^a μmol g⁻¹ dry weight.^b Conley (1997).

Amazon River along the dispersal system (Fig. 12). The incongruent nature of K vs. Si release during acid/alkaline reactions and the relative importance of operational pools are demonstrated by both the absolute magnitude of the acid and alkaline pools and the relative slopes (dK/dSi) of the relationships. The geometric mean regression slopes (dK/dSi) across the delta topset are 0.39 (K-HCl/Si-HCl), 0.12 (Alk-K/Si-Alk), and 0.19 mol mol⁻¹ (ΣK/ΣSi). The Macapá (riverbed) and river mouth samples (SJ-23) are not included in these calculations, although they lie on or close to overall trends. Those two sites had little

or no difference between the operational BSi and Si-Alk pools (i.e., most alkaline leachable Si was unaltered biogenic SiO₂) and small K-HCl/ΣK. The K-HCl/ΣSi ratio down core at station OST-2 is 0.17 mol mol⁻¹, comparable to that found in surface sediment between sites (Fig. 13A). Similarly, the down-core K-HCl/ΣSi slope in mobile muds off Amapá is ~0.11 and ΣK/ΣSi ~0.17 (Fig. 13B). Because of the relatively small and nearly constant quantity of BSi present in delta sediments, subtraction of the BSi concentration from ΣSi does not greatly affect the calculated slopes of ΣK/ΣSi. These slopes correspond closely to the K/Si ratio found in authigenic clays and altered diatom material obtained in both the field and in laboratory experiments (0.11–0.17; Table 1).

Table 3. Estimated reactive Si burial rates in the Amazon Delta.

Region ^a	Area (10 ¹³ cm ⁻²)	Accumulation rate ^a (g cm ⁻² yr ⁻¹)	Stations	ΣSi (μmol Si g ⁻¹)	ΣSi Burial (Tmol Si yr ⁻¹)
1	3.7	4.81	OST-3; Gas Site	412	0.0733
2	19.96	1.38	OST-1, 2; RMT-2, 3	267	0.0735
3	33.27	0.34	RMT-1	185	0.0209
4	3.42	0.17	SJ96-22	284	0.00165
Total	60.35				0.17

^a After: Showers and Angle (1986); Kuehl et al. (1986).

4.5.3. General Spatial Patterns in Reactive Sedimentary Si

Operational BSi concentrations show only minor spatial variation over the Amazon delta (DeMaster et al., 1983; Table 2), whereas mild acid leachable Si (Si-HCl) and Si-Alk increase progressively away from the Amazon River across the delta along the dispersal system by factors of ~4–5× (Figs. 12 and 14). The differences between the Si-Alk and BSi operational pools also increase regularly from ~0–2 in the Amazon riverbed (Macapá) and at the river mouth (SJ-23), to ~203

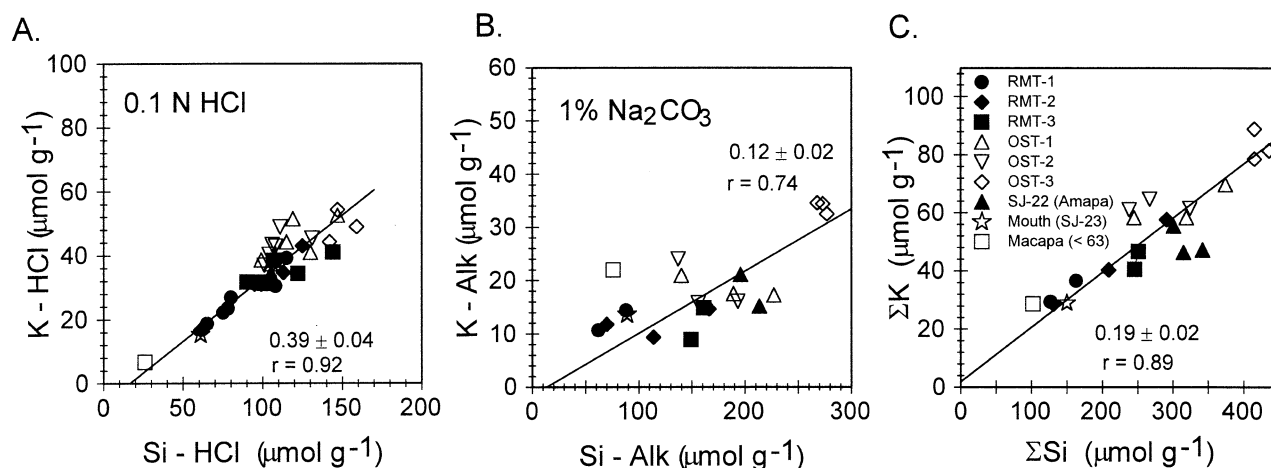


Fig. 12. The K^+ released during mild acid leach correlates strongly with reactive Si pools in delta deposits. Mild acid releases $\sim 70\%$ of the total K^+ released by the combined acid + alkaline leach, whereas the alkaline BSi leach alone releases $\sim 50\%$ of the combined value in < 2 h. (A) Mild acid leachable K-HCl vs. acid leachable Si-HCl in surface deposits (upper 15 cm). (B) Mild alkaline leachable K-Alk vs. alkaline leachable Si-Alk. (C) Total reactive K (K-HCl + K-Alk) vs. total reactive Si (Si-HCl + Si-Alk). The geometric mean regression slopes are 0.39, 0.12, and 0.19 mol mol $^{-1}$ respectively ($r^2 = 0.92, 0.55, \text{ and } 0.79; p < 0.001$).

$\mu\text{mol g}^{-1}$ at OST-3, the most distal delta site (Figs. 11 and 14). As noted previously, only small analytical differences between BSi and Si-Alk are found for kaolinite, montmorillonite, and illite clay standards. The total reactive ΣSi pool reaches $412 \pm 31 \mu\text{mol Si g}^{-1}$ in surface sediment at OST-3 compared with a measured BSi of $33 \pm 13 \mu\text{mol Si g}^{-1}$. The inshore Amapá site, SJ96-22 (7 m depth), has comparable concentrations to topset site OST-2.

4.5.4. Reactive Si Distributions

There is little regular variation with depth in the average concentrations of the different reactive Si pools at any given delta site (Fig. 15). Exceptions are found in isolated intervals of particular cores (e.g., OST-2; Relict Gas Site; SJ96-22) and at the base of RMT-2. The former sites underlie regions subject to plankton blooms (DeMaster et al., 1996) and diatoms can be concentrated in occasional layers. The latter site lies within a corridor of interlayered sands and muds where grain size effects and sorting influence distributions (Kuehl et al., 1986). At RMT-2 (PC 4228) and Gas Site (PC 4221), 1-h alkaline leaches rather than time series intercepts from full 7–8 h time series were used to calculate the Si-Alk concentrations. Experiments showed that 1-h values were 0.87 ± 0.05 that derived by extrapolation to the intercepts of the time series. All analytical Si-Alk values were thus corrected upwards by a factor 1.15 at these two sites only (correction insignificant on scale of figure).

The concentrations and the largely depth independent patterns of reactive Si pools found at the Amapá proto-mud wave site, station SJ96-22 (Fig. 16A), are similar to the delta topset sites, particularly OST-2. The ΣSi , Si-Alk, and Si-HCl (18 h) off Amapá average 284 ± 54 , 177 ± 36 , and $107 \pm 14 \mu\text{mol Si g}^{-1}$ respectively. BSi (not shown) averages $77 \pm 37 \mu\text{mol Si g}^{-1}$. There is a hint of slightly higher reactive Si on average in the upper ~ 40 cm relative to underlying material. Sediment from selected depth intervals was size fractionated by wet sieving ($>63 \mu\text{m}$, $<125 \mu\text{m}$) and leached to examine the

relative operational behavior and potential contribution of whole, relatively unaltered diatom frustules (A.I. ~ 0.1 ; Fig. 7). Biogenic particles dominate the coarse size fractions in these muds. The frustule-rich size fractions were extremely high in reactive Si relative to bulk sediment (Fig. 16B). The ratio of Si-Alk/BSi in the coarse fraction is ~ 1 in surface sediment, whereas the ratio in bulk sediment, which includes accumulated fragmented material, is ~ 2 .

5. DISCUSSION

5.1. Forms of Sedimentary Biogenic Silica

5.1.1. Alteration of Siliceous Particles

Direct examinations of Amazon delta sediments demonstrate multiple forms of sedimentary biogenic silica or its diagenetic derivatives. In addition to relatively unaltered biogenic silica such as whole or corroded diatom frustules, a variety of altered particles are present. The two major classes of alteration products are: a) cation-rich aluminosilicate coatings on siliceous frustules and tests; and b) complete alteration of frustules to authigenic aluminosilicates. The metal-rich coatings are apparently similar to Al-enriched diatom frustules found by Van Bennekom et al. (1989) in Zaire River fan sediments but are also highly enriched in Fe (Fig. 4). Authigenic aluminosilicates are often K, Fe-rich and dominated by 7 and 10.2–11 Å forms (e.g., Fig. 6; Michalopoulos et al., 2000). Within the completely altered particle group, two major subclasses can be identified: i) particles that comprise primarily authigenic aluminosilicate material locally replacing biogenic silica, and ii) composite pseudomorphs consisting of authigenic clay and agglutinated sedimentary matrix material (Figs. 2 and 3). Completely altered diatom frustules and comparatively fresh, unaltered diatoms comprise end-members of a spectrum of particles that have intermediate degrees of conversion to aluminosilicates. Many of these intermediate stages form rapidly (several months to years)

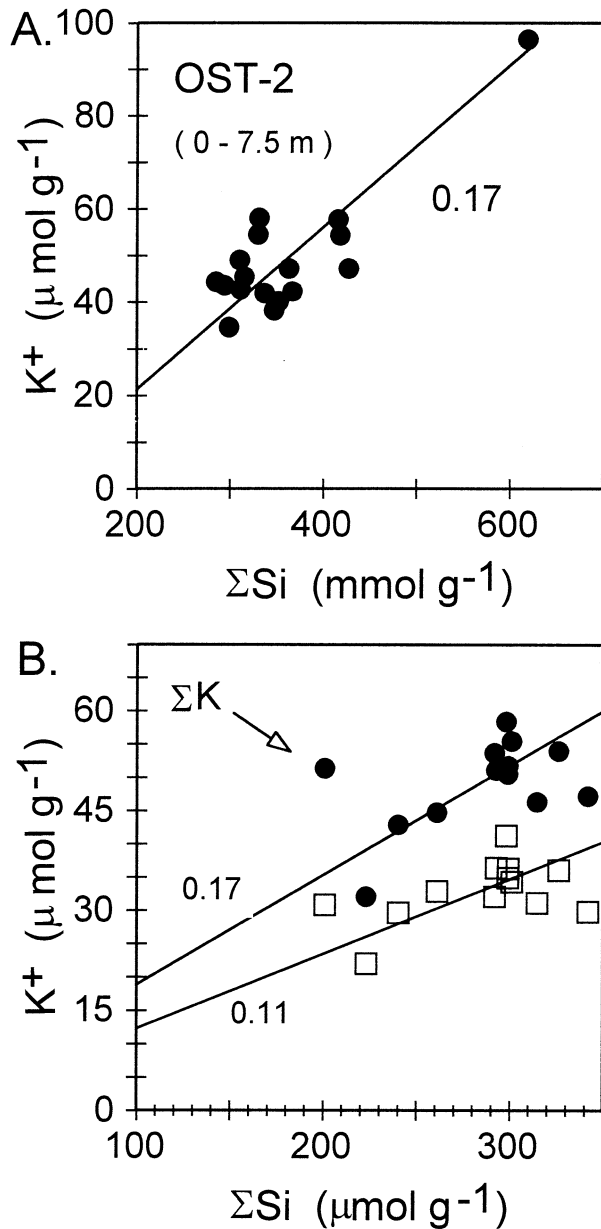


Fig. 13. (A) Acid leachable K^+ vs. total reactive Si down core at OST-2. Geometric mean slope = $0.17 \text{ mol mol}^{-1}$ ($r^2 = 0.71$, $p < 0.001$). (B) Acid leachable K^+ (K-HCl) and total leachable ΣK (acid + alkaline) vs. total reactive Si down core at Amapá proto-mudwave station SJ96-22. The geometric mean slopes are 0.11 ($r^2 = 0.25$; $p = 0.08$) and $0.17 \text{ mol mol}^{-1}$ ($r^2 = 0.23$; $p = 0.1$) respectively.

when diatom frustules are incubated experimentally in otherwise unamended Amazon delta sediments (Michalopoulos et al., 2000).

Microscopic observations show that diatom frustules can either maintain their initial morphology during alteration, disintegrate into recognizable frustual components, or completely fragment (Fig. 17). Disintegration is presumably caused by a combination of changes in the physical properties of the altered frustules and intense physical reworking. As exemplified by the multiple forms of diagenetic Si, the physically reworked zone consists of a complex spectrum of alteration products brought

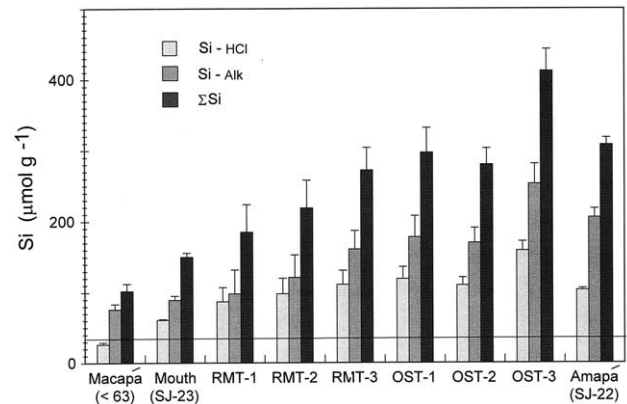


Fig. 14. Variation in the relative pools of reactive Si in surface deposits ($\sim 15 \text{ cm}$) from the Amazon River mouth across the delta and along the dispersal system. A regular increase occurs in all reactive pools but BSi. The average BSi measured previously in delta surface sediments is indicated as the horizontal line at $\sim 33 \mu\text{mol g}^{-1}$ (DeMaster et al., 1983).

together physically at various stages of reaction and preservation. Overall, the mobile surface zone of Amazon shelf deposits acts as a massive diagenetic batch reactor with periods of reworking–material exchange alternating with periods of relative stability and obvious net reaction (e.g., Fig. 8A; Aller et al., 1996; Aller, 1998). Surface deposits temporarily incorporate new reactive siliceous debris, sometimes into distinct layers, during net depositional events, while fragmenting and disseminating a portion of the previously formed authigenic aggregates into the general sediment matrix during remobilization. Based on simple division of the overall mass of sediment in the mobile zone and the delivery rate of sediment to the delta (Kuehl et al., 1986), the average residence time of particles in the reworked zone is roughly 30 yr. Because of exposure and erosion of deeply buried material as the mobile zone is reworked, however, older material can also be periodically reincorporated (e.g., average ^{14}C age of the mobile zone C_{org} is $\sim 2\text{--}3 \text{ Kyr}$; Kuehl et al., 1986; Sommerfield et al., 1995).

The discrete FeS-rich black layers that are found within the surface mobile zone and underlying relict ($> 100 \text{ yr}$) deposits represent pulsed inputs of fresh diatoms and other planktonic debris that are entrained and rapidly decomposed as sediment is reworked by currents and redeposited locally (Fig. 7). In the surface mobile deposits, these Fe-sulfide rich layers are usually destroyed and largely reoxidized during reworking events (\sim seasonally) but provide a short-term means of tracking the diagenetic behavior of specific reactive material. The alteration indexes of diatoms in the Fe-sulfide rich layers are $\sim 0.1\text{--}0.2$ in the mobile zone and very close to 1 at depth (Fig. 5C). These patterns demonstrate not only substantial diagenetic alteration on the short time scale of seasonal sediment reworking (A.I. $\sim 0.1\text{--}0.2$), but also the potential for complete conversion and lack of fragmentation if reactive material escapes the mobile surface region. The number of recognizable diatoms in bulk sediment decreases by orders of magnitude below the mobile zone, however, showing that most altered material is fragmented and disseminated before final burial (Fig. 7B). The relative constancy of operational pools of reactive Si in both the mobile and relict sediment region at most sites across the delta

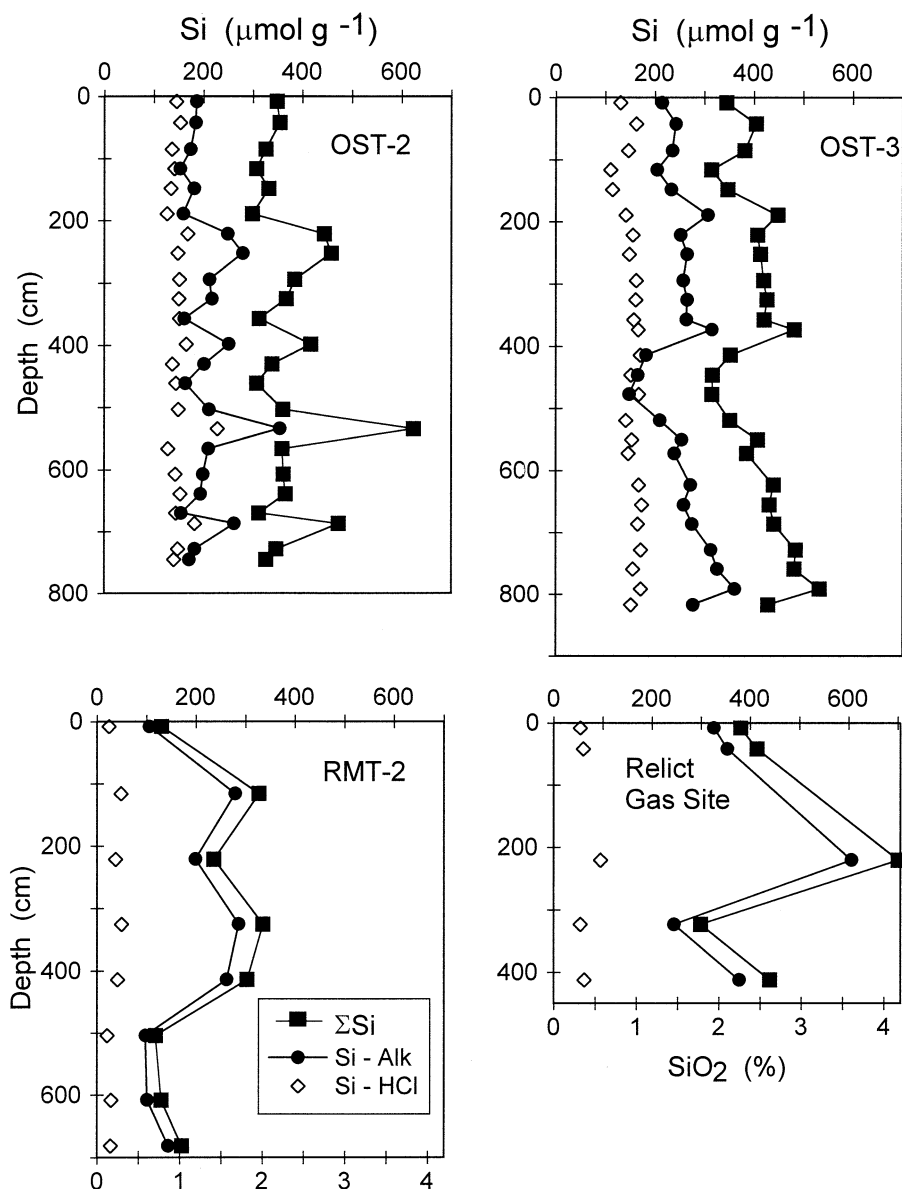


Fig. 15. Down core distributions of solid reactive Si pools at OST-2, OST-3, RMT-2, and the Relict Gas Site. Except for isolated intervals, concentrations are relatively constant at each site and reflect the dominant role of the mobile surface layer in mediating diagenesis. Average ΣSi are 370 ± 73 , 407 ± 57 , 218 ± 87 , and $446 \pm 152 \mu\text{mol Si g}^{-1}$ at OST-2, OST-3, RMT-2, and the Relict Gas Site (4221) respectively.

indicates that despite extensive fragmentation and loss of most distinct biogenic particles, the integrated diagenetic reaction products are essentially conserved and largely formed within the surface mobile layer (Figs. 7, 15, 16).

5.1.2. Diagenetic Microenvironments

The pyrite-filled diatoms (framboids $\geq 10 \mu\text{m}$ diameter) and diagenetic composite grains demonstrate that upon deposition, diatom cells acted as microenvironments for sulfate reduction (Figs. 2 and 3; Berner, 1970; Raiswell et al., 1993; Wilkin and Barnes, 1997). Metal, not sulfate, reduction typically dominates net diagenetic properties in the upper few meters of Amazon shelf deposits (Aller et al., 1986, 1996). As a consequence, the

average Fe-sulfide content in these deposits is much lower than most marine sediments of equivalent C content and metabolic activity (Aller et al., 1986; Aller and Blair, 1996). The presence of black, FeS-rich layers and individual pyrite-filled pseudomorphs indicates that on a local scale, net sulfate reduction can be important. Black laminae are $\sim 0.2\text{--}2 \text{ cm}$ thick and contain, in addition to abundant diatom pseudomorphs, relatively high concentrations of acid volatile sulfide (AVS $\sim 25\text{--}50 \mu\text{mol S g}^{-1}$), comparatively high total sulfur content ($\Sigma\text{S} \sim \text{AVS} + \text{pyrite} \sim 35\text{--}85 \mu\text{mol S g}^{-1}$), and authigenic carbonate minerals (Michalopoulos and Aller, 1996).

The close association of the products of organic matter decomposition and the products of Si-alteration in microenvi-

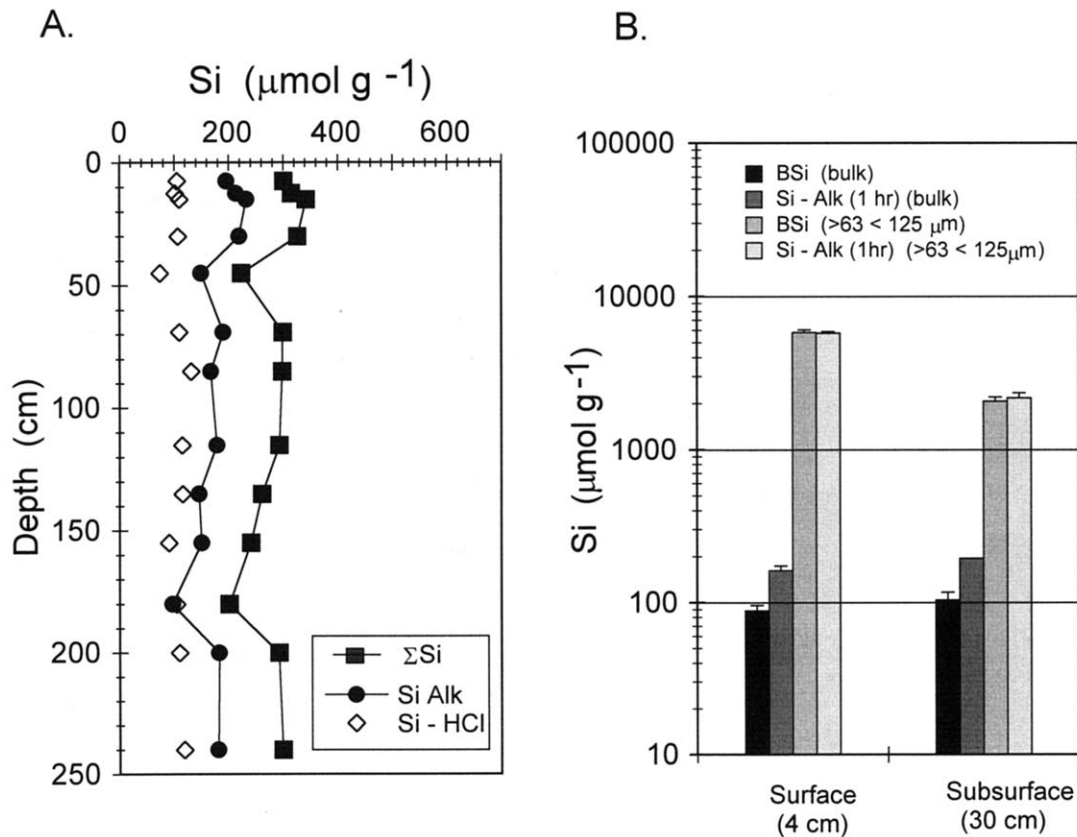


Fig. 16. (A) Down core distributions of solid reactive Si pools at Amapá site SJ96-22 demonstrate that preserved Si diagenetic patterns similar to the delta extend to mobile muds further along the dispersal system. Average ΣSi is $284 \pm 54 \mu\text{mol Si g}^{-1}$. (B) Relative reactive Si concentrations in bulk sediment and in the diatom enriched fine sand fraction in surface sediment (63–125 μm ; represents <0.4% weight total sediment grain size fraction). Pure opal would be $\sim 15 \text{ mmol Si g}^{-1}$ ($\text{SiO}_2 \cdot 0.4\text{H}_2\text{O}$). The relatively low alteration index (~ 0.1) of whole diatoms in the surface deposit (Fig. 7) is reflected in similar extraction by either mild alkaline or mild acid–mild alkaline, whereas fragmented, altered material in the bulk sediment shows differential extraction. The difference between BSi and Si-Alk shows a slight increase with depth in the coarse, diatom-rich fraction.

ronments and sedimentological structures (laminae) suggest similar timescales of formation. Fresh plankton typically decomposes on timescales of several weeks to months (Middelburg et al., 1993), and mobile layer sediment structure is formed and destroyed seasonally. In some cases we have found evidence that these diagenetic reactions may interact at the microenvironmental scales involved, also suggestive of contemporaneous processes. Diatom frustules with pyrite centers sometimes have lower Fe concentrations in authigenic silicate coatings than residual frustules lacking pyrite fill (e.g., Fig. 5). Competition for Fe^{+2} during formation of Fe-sulfides and authigenic silicates may locally inhibit Fe incorporation in the latter.

5.2. General Indicators of Authigenic Aluminosilicate Formation

5.2.1. Pore Water Solute Patterns

In addition to direct observation of particle properties, a range of pore water solute distributions imply extensive and rapid authigenic clay formation throughout the Amazon delta. Concentration gradients of potential reactants involved in alu-

minosilicate formation (K, Mg, Si, F) are formed and maintained despite frequent reworking and exchange of the surface ~ 0.5 – 2 m of delta topset deposits (Figs. 8 and 9; Aller et al., 1986, 1996; Mackin and Aller, 1986; Mackin et al., 1988; Rude and Aller, 1994). Stoichiometric and solute flux relationships modeled from dissolved K, Al, and F gradients in the mobile zone are consistent with K- and Fe-rich clay mineral formation (Mackin and Aller, 1986; Rude and Aller, 1994; Michalopoulos and Aller, 1995). For example, diffusive flux ratios of F^-/K^+ were ~ 6 – 17 mmol mol^{-1} along OST, close to the molar range reported for well-crystallized glauconites (28 – $100 \text{ mmol mol}^{-1}$) and authigenic clays formed in the laboratory (21 mmol mol^{-1}) (Rude and Aller, 1994; Michalopoulos and Aller, 1995). Previous studies of solid-phase compositions have also demonstrated removal of K^+ by reaction with weathered clays or authigenesis in Amazon River-derived sediments (Eisma and van der Marel, 1971). Mg^{2+} is incorporated into both authigenic carbonate and clay phases (Aller et al., 1986; Rude and Aller, 1989; Michalopoulos and Aller, 1996). The patterns of dissolved Si fluxes from or into bottom sediments (Michalopoulos and Aller, 1995; DeMaster and Pope, 1996; Shiller,

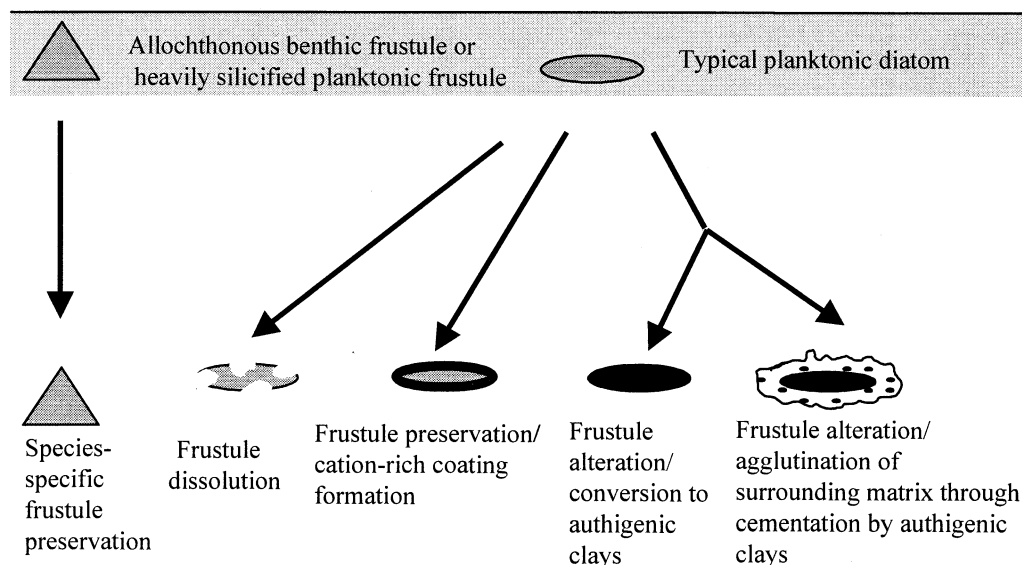


Fig. 17. Interpretive schematic diagram illustrating the multiple fates and coexisting classes of biogenic silica in Amazon delta deposits.

1996), and the magnitude of terminal dissolved Si concentrations (typically $\sim 50\text{--}450\ \mu\text{M}$), well below the solubility of opaline silica, also imply aluminosilicate formation (Figs. 8 and 9; Mackin, 1987; Michalopoulos and Aller, 1995). Gradients in all cases are highest in the upper 0.5–2 m, decreasing at depth, indicating that reaction rates are greatest within the mobile zone (e.g., Figs. 8 and 9).

5.2.2. Reactive K and Si Relations

The labile K and Si released during successive mild acid–mild alkaline extractions of sediment show highly coherent relationships both spatially across the delta and within cores at specific sites (Figs. 12 and 13). The inferred average stoichiometry of reactive $\Sigma\text{K}/\Sigma\text{Si} \sim 0.17\ \text{mol mol}^{-1}$ extracted from the delta deposits is far higher than that found in Amazon River suspended material (0.05–0.07; Martin and Meybeck, 1979; Sholkovitz and Price, 1980) and is indistinguishable from the average K/Si ratio measured in altered portions of diatoms in both delta sediments and from experimental incubations (Table 1). It is also within the general range expected for illite, glauconite, and celadonite (~ 0.2) (Velde, 1992). As noted earlier, standard clays and Amazon River sediment release smaller amounts of reactive K and Si than Amazon delta deposits and differ substantially from delta deposits in the relative importance of operational reactive pools (Table 2).

The overall spatial patterns of reactive K and Si imply a generally increasing abundance of diagenetic alteration products across the delta, with the highest concentrations found furthest offshore at OST-3 (Figs. 12 and 14). Water column diatom production increases along the same overall path, consistent with possible increasing input of biogenic Si to bottom deposits (DeMaster et al., 1996). Sholkovitz and Price (1980) noted also a slight increase in bulk K/Al in suspended matter across the shelf, and inferred an increased incorporation of K into biogenic debris. These changes in reactive K and Si across

the delta and along the dispersal system might reflect in whole or in part, a fortuitous combination of mineralogical and grain-size changes along transport paths. Sediment does tend to become more fine grained and slightly enriched in montmorillonite along the dispersal system but is progressively *depleted* in illite ($10\ \text{\AA}$), the most K-rich clay (Gibbs, 1977; Kuehl et al., 1986, 1995). There are also no major variations down core in grainsize, mineralogy, or pore water salinity at sites away from the river mouth (e.g., OST-2; Fig. 13A).

Increasing reactive K^+ may in part reflect salinity increases and adsorption. Most salinity variation in bottom water occurs inshore of RMT-2 and OST-2, however, so no salinity-based pattern alone would be expected at or seaward of those sites. Cation exchange capacity can reach up to $\sim 400\ \mu\text{eq g}^{-1}$ in the finest fractions ($< 2\ \mu\text{m}$) of Amazon River sediment of which $\sim 8\%$, or up to $\sim 32\ \mu\text{mol K g}^{-1}$, is occupied by K^+ in seawater at pH 8.2 (Sayles and Mangelsdorf, 1979). This estimate of adsorbed K^+ is an extreme upper limit because the pH of delta pore waters is generally ~ 7.2 , dissolved Mn^{2+} is $\sim 0.1\text{--}0.2\ \text{mM}$, dissolved Fe^{2+} is $\sim 0.5\text{--}1\ \text{mM}$, dissolved NH_4^+ reaches 3–4 mM, and deposits need not be composed entirely of particles having the highest exchange capacity, all factors further minimizing adsorbed K^+ (e.g., displacement by H^+ , NH_4^+ , Mn^{2+} , Fe^{2+}).

Detrital mineral components such as high-charge illite could fix K upon interaction with seawater (Eisma and Van der Marel, 1971; Hover et al., 2002). Indications for K fixation have been shown in laboratory manipulations of Amazon deltaic sediments after boiling sediment with K-saturated solutions for 8 h (Eisma and Van der Marel, 1971). In addition, K uptake through exchange reactions is likely to take place in high-charge smectite upon interaction with seawater and during burial in deltaic sediments, such as in the Mississippi delta (Hover et al., 2002). K-enriched detrital illite and smectite are potential sources for the labile K pool observed in the acid

extractions, and fixed K in illite is a potential source of K released during the alkaline extraction. However, the release of K from these pools is unlikely to account for the nearly constant stoichiometry of total labile K and Si released during operational extractions. In the absence of authigenic aluminosilicate formation, a simultaneous increase in K uptake by the detrital components in fortuitous proportion to increases in labile biogenic silica in the sediments would be required to explain the observed trends. Thus, the within- and between-site K/Si relationships (Figs. 12–14), the magnitude of reactive K ($\sim 20\text{--}100 \mu\text{mol K g}^{-1}$), the release of all K under operational conditions releasing the labile Si fraction, and the closely constrained stoichiometric ratios throughout the system are most consistent with a dominance of clay authigenesis rather than K-fixation or depositional control.

5.2.3. Reactive Si

The extraction of standard clays together with the bulk mineralogy of deposits indicate that there should be only a minor contribution of well-crystallized material to the operational reactive Si pools. The timing and magnitude of Si (and K) release during the mild acid treatment step also indicate that Si is unlikely to come predominantly from dissolution of Fe-oxides. Visual evidence during leaching of altered diatom frustules demonstrates directly that while the two-step mild acid + mild alkaline procedure used here is far more efficient at extracting altered material than the mild alkaline leach alone, it may still be a relatively conservative measure. As justified in detail in the method and results sections, we think that the combined mild acid (18 h)–mild alkaline procedure is the best operational compromise presently available to estimate biogenic silica and its early diagenetic products. The sum of the Si derived initially from the two-step extraction ($\Sigma\text{Si} = \text{Si-HCl} + \text{Si-Alk}$) is assumed here to represent the reactive Si pool including biogenic SiO_2 and labile authigenic derivatives. Given this assumption and the conclusion that crystalline minerals should not dominate the analytical signal, the ratio $(\Sigma\text{Si} - \text{BSi})/\Sigma\text{Si}$ should largely reflect diagenetic alteration of the reactive Si pool. This ratio increases regularly and progressively across shelf and along the dispersal system from the Amazon River bed at Macapá ($\sim 0.31\text{--}0.5$), the river mouth station SJ96-23 (~ 0.51), inshore Amapá SJ96-22 (0.75), to offshore OST-3 (0.92). If the Si released by mild acid is not included (a more conservative analytical assumption), the difference ratio: $[(\text{Si-Alk}) - \text{BSi}]/(\text{Si-Alk})$, increases from $-0.08\text{--}0.33$ (Macapá), 0.18 (SJ96-23), 0.63 (Amapá), to 0.83 (OST-3). These patterns suggest that both the magnitude of reactive Si derived from biogenic debris and the extent (%) of its alteration increase across the delta and along the dispersal system.

5.3. Rates of Diagenetic Alteration and Clay Formation

A variety of evidence indicates that the alteration of biogenic silica and conversion to clays is a rapid process in the Amazon delta, with characteristic timescales of months to a few years. The most direct and irrefutable evidence of the potential for rapid reactions comes from laboratory incubations of unamended Amazon delta sediments. Experiments where cultured

diatoms were inserted into deltaic muds resulted after 20–23 months in complete conversion of frustules into a range of cation-rich silicates, including K-Fe-rich clay minerals (Michalopoulos et al., 2000). Comparable experiments with additional natural particle surfaces (quartz, Fe-oxide, kaolinite, glass) demonstrated readily detectable precipitation of equivalent clay phases on timescales of $\sim 1\text{--}3$ yr (Michalopoulos and Aller, 1995).

The black, authigenic mineral-rich laminae, which are related to episodic biogenic silica delivery, are present in mobile zone sediment intervals throughout the delta (e.g., OST transect). It is certain that the secondary minerals in these seasonally reworked layers are autochthonous products of early diagenesis and thus the associated altered diatoms pseudomorphs have been formed over time scales of months to years, and are not simply recycled during erosion/redeposition. At station SJ96-22, totally altered diatoms are readily found in layers within the upper 20 cm and represent $\sim 10\%$ of recognizable frustules. Diagenetic modeling of pore water solute distributions and measured organic matter decomposition rates show that these surface-most sediments were rapidly and recently deposited before sampling (<months; unpublished data).

Pore water gradients and non-steady-state changes allow rough estimates of rates of silica alteration or clay formation. For example, at OST-2 the change in K^+ concentration over the upper ~ 1 m from August to May is at least ~ 2.2 mM, and may have involved deeper regions (Fig. 8A,B). Assuming that this change is a seasonal phenomenon, the average K^+ uptake rate over the upper 1 m is $\sim 220 \mu\text{mol cm}^{-2} \text{yr}^{-1}$ or $\sim 2.8 \mu\text{mol g}^{-1} \text{yr}^{-1}$ (average porosity of ~ 0.7 ; particle density of 2.6 g cm^{-3}). Because of the large spatial scale (~ 1 m) and short time (< 1 yr) involved, the mobile sediment layer as a whole can be treated as approximately closed with respect to diffusion during periods of stability. At the calculated rate ($2.8 \mu\text{mol g}^{-1} \text{yr}^{-1}$), it would take $\sim 7\text{--}36$ yr to add the quantity of labile K ($20\text{--}100 \mu\text{mol K g}^{-1}$) released from the operational extractions (Figs. 12 and 13). Further assuming a $\Sigma\text{K}/\Sigma\text{Si}$ authigenic product ratio of $0.17 \text{ mol mol}^{-1}$, the equivalent Si alteration or clay formation rate would be $\sim 15 \mu\text{mol Si g}^{-1} \text{yr}^{-1}$ (or $\sim 1.2 \text{ mmol Si cm}^{-2} \text{yr}^{-1}$ over upper ~ 1 m), capable of transforming $\sim 300 \mu\text{mol Si g}^{-1}$ in ~ 20 yr. These timescales are remarkably similar to the average particle residence time (~ 30 yr) estimated earlier for material in the mobile zone and are also consistent with the conclusion that most diagenetic changes take place in the mobile layer.

Rude and Aller (1994) estimated a F^- uptake rate by Amazon delta sediments of $\sim 7.8 \mu\text{mol F cm}^{-2} \text{yr}^{-1}$, using diffusive flux models, sediment incubations, and differences between the average F content of Amazon River and Delta deposits along RMT and OST (Fig. 1). Operational solid-phase extractions indicated that most F^- was consumed during authigenic silicate formation not by carbonate fluorapatites. The average F/K ratio in authigenic clays formed in laboratory incubations of Amazon delta sediment is $\sim 21 \text{ mmol mol}^{-1}$, and in the lower range reported for well-formed glauconites (Michalopoulos and Aller, 1995). Assigning the entire F^- flux to authigenic clay formation of equivalent composition implies a K^+ flux of $\sim 370 \mu\text{mol K cm}^{-2} \text{yr}^{-1}$. This estimate is in the range of the simple closed system calculation made previously

for a ~1-m-thick mobile layer (a conservative thickness for OST-2).

Therefore multiple independent methods of constraining biogenic silica alteration rates provide a consistent picture of very rapid authigenic silicate formation (months, years). Visual observations, instrumental measures of elemental compositions, pore water distributions, operational extractions, laboratory experiments, and estimates of the quantities formed are mutually supportive, and indicate that the operational reactive ΣSi pool is formed diagenetically and derived from biogenic silica. Although it is conceivable that alternative explanations could be given to any single observation, for example, differential transport of a poorly crystalline, K-rich soil component could account for spatial patterns, the most parsimonious conclusion is authigenesis.

5.4. Availability and Storage of Reactive Si

5.4.1. Si as a Limiting Reactant

We hypothesized that the availability of reactive silica may be the primary factor limiting production of authigenic aluminosilicates in Amazon delta sediments, where highly weathered Fe, Al-oxide rich debris is abundant (Michalopoulos and Aller, 1995). The occurrence of sedimentary silica in these sediments is consistent with this Si limitation. Only a small proportion of the total reactive Si pool remains unaltered and extractable by mild alkaline leaches (Fig. 11; Table 2). The diatom alteration index demonstrates that virtually 100% of recognizable diatoms are eventually converted (Fig. 7). The fact that authigenic clays form diatom pseudomorphs indicates that SiO_2 can be the primary substrate and site of formation, and that Si need not be transported and precipitated remotely at the site of another limiting reactant. The lack of residual biogenic Si during conversion of diatoms in laboratory incubations also implies that other reactants are in relative excess.

Availability of reactive silica may limit or closely control clay formation in other deltaic systems. For example, in Mississippi Delta sediments the occurrence of authigenic Fe-rich aluminosilicate (glauconite) has increased in surface sediments over the last ~50 yr of deposition (Nelsen et al., 1994). During the same period, the amount of biogenic silica stored in these sediments also increased due to increased supply of nutrients by the river and enhanced primary production in the coastal shelf waters due to eutrophication (Turner and Rabalais, 1994). The timescales observed for glauconite formation in Mississippi delta sediments are of the order documented in Amazon delta deposits. Even though there is no direct documentation for conversion of diatoms to clays at the Mississippi site, the correlation between increased biogenic silica supply and the formation of green clays suggests that the two are linked. These inferences support the concept that deltaic depositional systems in general have the capacity for substantial conversion of biogenic silica and storage as derivative minerals.

In many recent studies of biogenic Si cycling in sediments, the interdependence between reactive Al and early diagenesis of biogenic silica has been invoked to explain pore-waters with Si concentrations below those predicted from opaline Si solubilities (Mackin, 1986; Mackin and Aller, 1989; Van Cappellen and Qiu 1997a; King et al., 2000; Dixit et al., 2001). It is likely

that within the marine realm there exists a continuum in the early diagenetic behavior of biogenic silica. The two end members of this spectrum can be represented by tropical deltaic settings such as the Amazon delta, and deep-sea siliceous sediments. The factor that controls the degree of biogenic silica conversion is the ratio of biogenic silica to other limiting reactive constituents (e.g., Al, Fe) that have as major sources the terrigenous material carried by rivers and atmospheric input (Aplin, 1993). In tropical deltaic sediments subjected to intense physical reworking and containing Al,Fe-oxide-rich weathered debris, the limiting factor is the availability of biogenic silica, whereas in deep-sea settings characterized by biosiliceous sediments (Van Cappellen and Qiu, 1997a) or in carbonate platform sediments (Mackin and Aller, 1989), the limiting factor is the availability of Al,Fe-oxide. Metalliferous deep-sea sediments near hydrothermal sources may also be reactive Si-limited (e.g., Bauer Deep; Johnson, 1976; Cole, 1985), and quite comparable to energetic tropical deltas.

5.4.2. Biogenic Silica Storage

The lack of conclusive evidence for the formation of authigenic clay minerals in the past has resulted in the omission of such a process in the construction of the elemental cycle of Si on the Amazon shelf and elsewhere (DeMaster et al., 1983; Ragueneau et al., 2000). For example, early estimates of the biogenic silica content of Amazon deltaic sediments measured an average content of BSi ~0.2% SiO_2 (~33 $\mu\text{mol Si g}^{-1}$) (DeMaster et al., 1983). The analytical BSi pool was assumed to represent the sedimentary form of stored biogenic Si. This concentration translates into a biogenic SiO_2 accumulation rate of ~0.03 Tmoles yr^{-1} . Subsequent estimates of storage have increased as the potential for aluminosilicate formation has been recognized (DeMaster and Aller, 2001). Based on a variety of self-consistent analytical, experimental, and field data, we have demonstrated here that the operational analytical reactive Si pool, ΣSi , represents a better estimate of the total quantity of biogenic Si and early diagenetic derivatives present in Amazon delta sediments. Most alteration of Si occurs in the surface mobile zone, which acts functionally as a diagenetic batch reactor. Local vertical gradients in reactive ΣSi concentration are thus minimized throughout most of the delta (Figs. 15 and 16). The quantity of ΣSi at specific sites varies regularly, however, across shelf and along the dispersal system (Fig. 14).

To estimate net ΣSi storage, we utilized regional contour maps of net accumulation rate on the delta and assigned average concentrations of reactive ΣSi to regions based on our sample stations (Kuehl et al., 1986; Showers and Angle, 1986). The highest net accumulation rates occur in the OST-3 region in close proximity to the scoured relict gas station (Fig. 1). The average down core concentration of ΣSi averages ~1.15 \times that found in the surface 15 cm where both measures are available, indicating that the two measures are not significantly different within error. Therefore, when a down core average was not available, the surface concentration was used (RMT-1, RMT-3, OST-1). The relict gas site (PC4221) was not used in budget calculations but the average value of ΣSi (446 $\mu\text{mol Si g}^{-1}$) is comparable to that at OST-3. A range of additional diagenetic indicators demonstrate that exposed relict deposits (>0.1–1 kyr

age) had initial diagenetic conditions similar to those in the modern surface mixed zone (Blair and Aller, 1995; Sommerfield et al., 1995; Aller et al., 1996; Zhu et al., 2002).

The total accumulation of reactive ΣSi is $\sim 1.7 \times 10^{11}$ mol Si yr^{-1} or $0.17 \text{ Tmoles yr}^{-1}$ (Table 2), and represents $\sim 22\%$ of the estimated Amazon River input of 7.67×10^{11} (DeMaster and Pope, 1996). This estimate is $\sim 5\text{--}6\times$ that based on operational BSi concentrations. The accumulation rate weighted average ΣSi in delta deposits is $296 \mu\text{mol Si g}^{-1}$, or $1.8\% \text{ SiO}_2$ (Table 2). This estimate is in good agreement with calculations from pore-water gradients and authigenic-mineral compositions indicating that $\sim 3\%$ by weight of Amazon delta sediments are authigenic clays ($\Rightarrow \sim 0.7\text{--}1.0\% \text{ SiO}_2$; Michalopoulos and Aller, 1995). It also agrees well with the range inferred by Shiller (1996) from water column box models. Globally, the Amazon contributes $\sim 14\%$ of the total riverine dissolved Si to the oceans (DeMaster and Pope, 1996; Tréguer et al., 1995). Tropical rivers contribute $\sim 74\%$ of the total riverine Si input to the oceans. Previous estimates for the uptake of riverine Si by tropical marine depositional systems give a value of $\sim 0.4 \text{ Tmoles yr}^{-1}$ based on an average trapping efficiency of $\sim 10\%$ (Tréguer et al., 1995). Extrapolating the minimum trapping efficiency of the Amazon ($\sim 22\%$) estimated in this study to all tropical river systems yields a burial of $\sim 0.9 \text{ Tmoles yr}^{-1}$ in these depositional environments, $2\text{--}3\times$ that previously assumed and $\sim 15\%$ of global biogenic Si burial.

5.5. Reverse Weathering and Elemental Cycling

Our present and previous findings demonstrate that significant quantities of biogenic silica are rapidly converted into cation-rich aluminosilicates in deltaic sediments, and imply that the availability of reactive silica in deltas is a major controlling factor. Although biogenic silica can be a critical reactant and a site of precipitation, other reactions may produce authigenic clays. In the Amazon delta sediments, for example, authigenic 7Å Fe-Mg rich clays and 10Å clays are also formed within Fe-oxide coatings over detrital sand grains (Rude and Aller, 1989). In addition, progressive dissolution/recrystallization of kaolinite has been proposed as a mechanism for formation of apparently comparable 7 and 10 Å Fe-rich clays in green peloids from the Zaire estuary, but over a much longer time period (Giresse et al., 1988; Amouric et al., 1995). More generally, suites of ~ 7 , 10 , and 14 Å Fe-rich clays are known to form authigenically in numerous marine shelf and slope environments, although the rate of their formation is inferred to be over much longer timescales ($>10^3\text{--}10^4 \text{ yr}$) than required in the present case, and they are not reported as widely disseminated components of deltaic mud deposits (Porrenga, 1967; Odin et al., 1988; Odin, 1990; Aplin, 1993).

The overall diagenetic reactions responsible for biogenic silica conversion to cation-rich Al,Si phases in the Amazon delta involve the mobilization of Al and Fe during early diagenesis, uptake of K (Li, Na ?), Mg, and F from seawater, and the addition of SiO_2 from diatoms or other reactive glass debris. Fe mobilization is partly the result of delivery of highly weathered material by the Amazon River, but is enhanced tremendously by reoxidation cycles during sediment reworking (Aller, 1998; Aller et al., 1986). The availability of abundant reactive Al-oxide is also the result of terrestrial weathering and riverine

inputs. The Si incorporated into the diatoms has its origin in silicate rocks on land, and the transport of the dissolved and reactive particulate Si to the ocean by rivers. Thus the conversion of biogenic silica (SiO_2) by reaction with detrital $\text{Al}(\text{OH})_3$, $\text{Fe}(\text{OH})_3$, and dissolved cations in seawater constitutes reverse weathering (*sensu* Mackenzie and Garrels, 1966). The elemental mass fluxes involved are significant. Estimates of F and K fluxes, for example, indicate that $7\text{--}10\%$ of the global river flux is consumed in the Amazon delta alone. The lack of consideration for reverse weathering processes in deltas suggests that global budgets for associated elements are inadequate.

6. CONCLUSIONS

Biogenic silica deposited in deltaic sediments of the Amazon River undergoes a variety of diagenetic alteration processes leading in large part to the formation of authigenic K-Fe-rich aluminosilicates. The general classes of stored biogenic silica include fresh siliceous particles (frustules), whole or partially dissolved diatoms, metal-coated silica, authigenic clay replacement, authigenic and matrix clay aggregates, and fragmented authigenic debris. Standard operational procedures designed to measure biogenic silica do not detect most diagenetic alteration products and substantially underestimate the quantity of reactive Si stored in the Amazon delta. A modified mild acid–mild alkaline procedure extracts the labile authigenic phases without significant contamination from well-crystallized clays or metal oxides. Because not all alteration products are included, these estimates remain minima.

Most ($\sim 90\%$) of the biogenic silica buried in Amazon delta sediments ($\sim 296 \mu\text{mol Si g}^{-1}$) is apparently converted into authigenic aluminosilicates. The new mineral phases and amorphous cation-rich aluminosilicate material formed are also responsible for the uptake of cations such as K and Mg, and other elements such as F. The K/Si ratio of labile authigenic phases is $\sim 0.17 \text{ mol mol}^{-1}$; $2\text{--}4\times$ higher than average Amazon River sediment. Early diagenetic alteration of Si occurs predominantly in the surface mobile zone, which is functionally a periodically fluidized batch reactor, and it takes $\sim 7\text{--}36 \text{ yr}$ to precipitate the quantity of authigenic material observed (e.g., $\sim 2.8 \mu\text{mol K g}^{-1} \text{ yr}^{-1}$). Deltaic sinks for silica and many other seawater solutes have been discounted in the majority of geochemical budgets in the past, implying that the burial of biogenic silica and uptake of major elements in continental margin environments may be substantially underestimated. In the case of the Amazon delta, biogenic Si is apparently the limiting reactant whereas in other depositional settings such as the Antarctic, reactive Al may limit alteration processes. Direct evidence for the rapid formation of authigenic aluminosilicate phases in tropical shelf muds and deltaic environments—the major modern sediment depocenters—demonstrates the need for incorporation of such processes in the construction of global elemental budgets.

Acknowledgments—Numerous people and organizations, both U.S. and Brazilian, aided this study at various times over the many years that field sampling, laboratory experiments, and analytical work included here were carried out. The AmasSeds project (1989–94) was headed by C. Nittrouer, D. DeMaster, and A. Figueiredo. We thank J. Mackin, P. Rude, N. Blair, H. Vigil, Q. Xia, C. Nittrouer, M. Allison, S. Kuehl, J. Aller, M. Green, S. Beame, E. Breuer, S. Dunn, M. Lima, and many

others for assistance at sea. Q. Xia, C. Panzeca, C. Heilbrun, and C. Rossi aided in the lab. Research in Amapá would not have been possible without our Brazilian colleagues S. Patchineelam, O. Silveira, A. Mendes, and J. Todorov. The captain and crews of the *R/V Islin* and *R/V Seward Johnson* were instrumental in the success of field sampling. We thank P. N. Froelich and D. J. DeMaster for critical reviews and suggestions (not all taken). This research was supported by NSF grant OCE9818574 and predecessors. Dedicated to our dear friend and colleague the late Qing Xia.

Associate editor: L. R. Kump

REFERENCES

- Alexander C. R. Jr., Nittrouer C. A., and DeMaster D. J. (1986) High-resolution seismic stratigraphy and its sedimentological interpretation on the Amazon continental shelf. *Cont. Shelf Res.* **6**, 337–358.
- Aller J. Y. and Todorov J. (1997) Seasonal and spatial characteristics of benthic communities on the Amazon shelf as indicators of physical processes. *Cont. Shelf Res.* **16**, 717–751.
- Aller J. Y. and Stupakoff I. (1996) The distribution and seasonal characteristics of benthic communities on the Amazon shelf as indicators of physical processes. *Cont. Shelf Res.* **16**, 717–752.
- Aller R. C., Blair N. E., Xia Q., and Rude P. (1996) Remineralization rates, recycling, and storage of C_{org} in Amazon Shelf sediments. *Cont. Shelf Res.* **16**, 753–786.
- Aller R. C., Mackin J. E., and Cox R. T. Jr. (1986) Diagenesis of Fe and S in Amazon inner shelf muds: Apparent dominance of Fe reduction and implications for the genesis of ironstones. *Cont. Shelf Res.* **6**, 263–289.
- Aller R. C. and Blair N. E. (1996) Sulfur burial on the Amazon shelf. *GeoMarine Lett.* **16**, 3–10.
- Aller R. C. (1998) Mobile deltaic and continental shelf muds as suboxic, fluidized bed reactors. *Mar. Chem.* **61**, 143–155.
- Allison M. A., Lee M. T., Ogston A. S., and Aller R. C. (2000) Origin of Amazon mudbanks along the northeastern coast of South America. *Mar. Geol.* **163**, 241–256.
- Amouric M., Parron M., Casalini C., and Giresse P. (1995) A (1:1) 7-Å Fe phase and its transformation in recent sediments: An HRTEM and AEM study. *Clays and Clay Min.* **43**, 446–454.
- Aplin A. C. (1993) The composition of authigenic clay minerals in recent sediments: Links to the supply of unstable reactants. In *Geochemistry of Clay-Pore Fluid Interactions* (eds. D. A. C. Manning, P. L. Hall, and C. R. Hughes), pp. 81–106. Chapman and Hall, London.
- Badaut D. and Risacher F. (1982) Authigenic smectite on diatom frustules in Bolivian saline lakes. *Geochim. Cosmochim. Acta* **47**, 363–375.
- Berner R. A. (1970) Sedimentary pyrite formation. *Am. J. Sci.* **268**, 1–23.
- Berner R. A. (1982) Burial of organic carbon and pyrite sulfur in the modern ocean: Its geochemical and environmental significance. *Am. J. Sci.* **282**, 451–473.
- Berner R. A. (1980) *Early Diagenesis: A Theoretical Approach*. Princeton University Press.
- Blair N. E. and Aller R. C. (1995) Anaerobic methane oxidation on the Amazon shelf. *Geochim. Cosmochim. Acta* **59**, 3707–3715.
- Cacchione D. A., Drake D. E., Kayen R. W., Sternberg R. W., Kineke G. C., and Tate G. B. (1995) Measurements in the bottom boundary layer on the Amazon subaqueous delta. *Mar. Geol.* **125**, 235–257.
- Calvert S. E. (1983) Sedimentary geochemistry of silicon. In *Silicon Geochemistry and Biogeochemistry* (ed. S. R. Aston), pp. 143–186. Acad. Press, London.
- Canfield D. E. (1989) Reactive iron in marine sediments. *Geochim. Cosmochim. Acta* **53**, 2483–2490.
- Cole T. G. (1985) Composition, oxygen isotope geochemistry, and origin of smectite in the metalliferous sediments of the Bauer Deep, Southeast Pacific. *Geochim. Cosmochim. Acta* **49**, 221–235.
- Conley D. J. (1998) An interlaboratory comparison for the measurement of biogenic silica in sediments. *Mar. Chem.* **63**, 39–48.
- Dasch E. J. (1969) Strontium isotopes in weathering profiles, deep sea sediments and sedimentary rocks. *Geochim. Cosmochim. Acta* **33**, 1521–1552.
- DeMaster D. J., Knapp G. B., and Nittrouer C. A. (1983) Biological uptake and accumulation of silica on the Amazon continental shelf. *Geochim. Cosmochim. Acta* **47**, 1713–1723.
- DeMaster D. J. (1981) The supply and accumulation of silica in the marine environment. *Geochim. Cosmochim. Acta* **45**, 1715–1732.
- DeMaster D. J. (1991) Measuring biogenic silica in marine sediments and suspended matter. In: *Marine Particles: Analysis and Characterization*. *Geophysical Monograph*. **63**, 363–367.
- DeMaster D. J. (2002) The accumulation and cycling of biogenic silica in the Southern Ocean: Revisiting the marine silica budget. *Deep-Sea Res. II* **49**, 3155–3167.
- DeMaster D. J., Smith W. O. Jr., Nelson D. M., and Aller J. Y. (1996) Biogeochemical processes in Amazon shelf waters: Rates and chemical distributions. *Cont. Shelf Res.* **16**, 617–643.
- DeMaster D. J. and Pope R. H. (1996) Nutrient dynamics in Amazon shelf waters: Results from AMASSEDS. *Cont. Shelf Res.* **16**, 263–289.
- DeMaster D. J. and Aller R. C. (2001) Biogeochemical processes on the Amazon Shelf: Changes in dissolved and particulate fluxes during river/ocean mixing. In *The Biogeochemistry of the Amazon Basin* (eds. M. E. McClain, R. L. Victoria, and J. E. Richey), pp. 328–357. Oxford Univ. Press, Oxford.
- Dixit S. and Van Cappellen P. (2002) Surface chemistry and reactivity of biogenic silica. *Geochim. Cosmochim. Acta* **66**, 2559–2568.
- Dixit S., Van Cappellen P., and van Bennekom A. J. (2001) Processes controlling solubility of biogenic silica and pore water build-up of silicic acid in marine sediments. *Mar. Chem.* **73**, 333–352.
- Dukat D. A. and Kuehl S. A. (1995) Non-steady state ^{210}Pb flux and the use of $^{228}\text{Ra}/^{226}\text{Ra}$ as a geochronometer on the Amazon continental shelf. *Mar. Geol.* **125**, 329–350.
- Eggemann D. W., Manheim F. T., and Betzer P. R. (1980) Dissolution and analysis of amorphous silica in marine sediments. *J. Sed. Petrol.* **50**, 215–225.
- Eisma D. and Van der Marel H. W. (1971) Marine muds along the Guyana coast and their origin from the Amazon Basin. *Contr. Miner. Petrol.* **31**, 136–140.
- Gehlen M., Beck L., Calas G., Flank A.-M., Van Bennekom A. J., and Van Beusekom J. E. E. (2002) Unraveling the atomic structure of biogenic silica: Evidence of the structural association of Al and Si in diatom frustules. *Geochim. Cosmochim. Acta* **66**, 1601–1610.
- Gehlen M. and van Rapphorst W. (1993) Early diagenesis of silica in sandy North Sea sediments: Quantification of the solid phase. *Mar. Chem.* **42**, 71–83.
- Geyer R. W., Beardsley R. C., Lentz S. J., Candela J., Limeburner R., Johns W. E., Castro B. M., and Soares I. D. (1996) Physical oceanography of the Amazon Shelf. *Cont. Shelf Res.* **16**, 575–616.
- Gibbs R. J. (1977) Clay mineral segregation in the marine environment. *J. Sed. Petrol.* **47**, 237–243.
- Giresse P., Wiewiora A., and Lacka B. (1988) Mineral phases and processes within green peloids from two recent deposits near the Congo River mouth. *Clay Minerals* **23**, 447–458.
- Heath G. R. and Dymond J. (1977) Genesis and transformation of metalliferous sediments from the East Pacific Rise, Bauer Deep and Central Basin, Northwest Nazca Plate. *Geol. Soc. Am. Bull.* **88**, 723–733.
- Hein J. R., Yeh H.-W., and Alexander E. (1979) Origin of iron-rich montmorillonite from the manganese nodule belt of the North Equatorial Pacific. *Clays and Clay Minerals* **27**, 185–194.
- Hover V. C., Walter L. M., and Peacor D. R. (2002) K uptake by modern estuarine sediments during early marine diagenesis, Mississippi Delta Plain, Louisiana. *J. Sediment. Res.* **72**, 775–792.
- Hurd D. C. (1973) Interactions of biogenic opal, sediment and seawater in the central equatorial Pacific. *Geochim. Cosmochim. Acta* **37**, 2257–2282.
- Johnson T. C. (1976) Biogenic opal preservation in pelagic sediments of a small area in the eastern tropical Pacific. *Bull. Geol. Soc. Am.* **87**, 1273–1282.
- Katamani A., Nobuhiko E., and Tréguer P. (1988) The dissolution of diatom ooze from the Antarctic area. *Deep-Sea Res.* **35**, 1195–1203.

- Kineke G. C. and Sternberg R. W. (1995) Distribution of fluid muds on the Amazon continental shelf. *Mar. Geol.* **125**, 193–233.
- King S. L., Froelich P. N., and Jahnke R. A. (2000) Early diagenesis of germanium in sediments of the Antarctic South Atlantic: In search of the missing Ge sink. *Geochim. Cosmochim. Acta* **64**, 1375–1390.
- Konhauser K. O., Fyfe W. S., and Kronberg B. I. (1994) Multi-element chemistry of some Amazonian waters and soils. *Chem. Geol.* **111**, 155–175.
- Kuehl S. A., Nittrouer C. A., and DeMaster D. J. (1986) Nature of sediment accumulation on the Amazon continental shelf. *Cont. Shelf Res.* **6**, 209–225.
- Kuehl S. A., Pacioni T. T., and Rine J. M. (1995) Seabed dynamics of the inner Amazon continental shelf: Temporal and spatial variability of surficial strata. *Mar. Geol.* **125**, 283–302.
- Kuehl S. A., Nittrouer C. A., Allison M. A., Faria L. E. C., Dukac D. A., Jaeger J. M., Pacioni T. D., Figueiredo A. G., and Underkoffler E. C. (1996) Sediment deposition, accumulation, and seabed dynamics in an energetic fine-grained coastal environment. *Cont. Shelf Res.* **16**, 787–815.
- Lewin J. C. (1961) The dissolution of silica from diatom walls. *Geochim. Cosmochim. Acta* **21**, 182–198.
- Ludwig W., Probst J. L., and Kempe S. (1996) Predicting the oceanic input of organic carbon by continental erosion. *Global Biogeochemical Cycles* **10**, 23–41.
- Mackenzie F. T. and Garrels R. M. (1966) Chemical mass balance between rivers and oceans. *Am. J. Sci.* **264**, 507–525.
- Mackenzie F. T., Ristvet B. L., Thorstenson D. C., Lerman A., and Leeper R. H. (1981) Reverse weathering and chemical mass balance in a coastal environment. In *River Inputs to the Ocean* (eds. J. M. Martin, J. D. Burton, and D. Eisma), pp. 152–187. UNEP-UNESCO, Switzerland.
- Mackin J. E. (1986) Control of dissolved Al distributions in marine sediments by clay reconstitution reactions: Experimental evidence leading to a unified theory. *Geochim. Cosmochim. Acta* **50**, 207–214.
- Mackin J. E. (1987) Relationships between Si, Al, and Fe deposited on filter-covered glass substrates in marine sediments and in suspensions of sediments and standard clays. *Mar. Chem.* **26**, 101–117.
- Mackin J. E. and Swider K. T. (1987) Modeling the dissolution behavior of standard clays in seawater. *Geochim. Cosmochim. Acta* **51**, 2947–2964.
- Mackin J. E., Aller R. C., and Ullman W. J. (1988) The effects of iron reduction and nonsteady-state diagenesis on iodine, ammonium, and boron distributions in sediments from the Amazon continental shelf. *Cont. Shelf Res.* **8**, 363–386.
- Mackin J. E. and Aller R. C. (1984) Diagenesis of dissolved aluminum in organic-rich estuarine sediments. *Geochim. Cosmochim. Acta* **48**, 299–313.
- Mackin J. E. and Aller R. C. (1986) The effects of clay mineral reactions on the dissolved Al distributions in sediments and waters of the Amazon continental shelf. *Cont. Shelf Res.* **6**, 245–262.
- Mackin J. E. and Aller R. C. (1989) The nearshore marine and estuarine chemistry of dissolved aluminum and rapid authigenic mineral precipitation. *Rev. Aquatic Sci.* **1**, 537–554.
- Martin J. M. and Meybeck M. (1979) Elemental mass-balance of material carried by major world rivers. *Mar. Chem.* **7**, 173–206.
- McManus J., Hammond D. E., Berelson W. M., Kilgore T. E., Demaster D. J., Ragueneau O. G., and Collier R. W. (1995) Early diagenesis of biogenic opal: Dissolution rates, kinetics, and paleoceanographic implications. *Deep-Sea Res. II* **42**, 871–879.
- Mead R. H., Dunne T., Richey J. E., Santos U., DeM., and Salati E. (1985) Storage and remobilization of suspended sediment in the lower Amazon River of Brazil. *Science* **228**, 488–494.
- Michalopoulos P. and Aller R. C. (1995) Rapid clay mineral formation in Amazon delta sediments: Reverse weathering and oceanic elemental cycles. *Science* **270**, 614–617.
- Michalopoulos P., Aller R. C. (1996) Early diagenetic carbonate minerals in Amazon delta sediments: Controls by depositional regime on formation, mineralogy and composition *Geological Society of America, abstracts*, p. 90.
- Michalopoulos P., Aller R. C., and Reeder R. J. (2000) Conversion of diatoms to clays during early diagenesis in tropical, continental shelf muds. *Geology* **28**, 1095–1098.
- Middelburg J. J., Vlug T., and van der Nat F. J. W. A. (1993) Organic matter mineralization in marine systems. *Global Planetary Change* **8**, 47–58.
- Milliman J. D. and Boyle E. A. (1975) Biological uptake of dissolved silica in the Amazon River estuary. *Science* **189**, 995–997.
- Milliman J. D. and Syvitski J. P. M. (1992) Geomorphic/tectonic control of sediment discharge to the ocean: The importance of small mountainous rivers. *J. Geology* **100**, 525–544.
- Moore W. S., DeMaster D. J., Smoak J. M., McKee B. A., and Swarzenski P. W. (1996) Radionuclide tracers of sediment-water interactions on the Amazon shelf. *Cont. Shelf Res.* **16**, 645–665.
- Mortlock R. A. and Froelich P. N. (1989) A simple method for the rapid determination of biogenic opal in pelagic marine sediments. *Deep-Sea Res.* **36**, 1415–1426.
- Nelsen T. A., Blackwelder P., Hood T., McKee B., Romer N., Alvarez-Zarikian C., and Metz S. (1994) Time-based correlation of biogenic, lithogenic and authigenic sediment components with anthropogenic inputs in the Gulf of Mexico NECOP study area. *Estuaries* **17**, 873–885.
- Nittrouer C. A., Curtin T. B., and DeMaster D. J. (1986) Concentration and flux of suspended sediment on the Amazon continental shelf. *Cont. Shelf Res.* **6**, 151–174.
- Odin G. S. (1990) Clay mineral formation at the continent-ocean boundary: The verdine facies. *Clay Minerals* **25**, 477–483.
- Odin G. S. and Frohlich F. (1988) Glaucony from the Kerguelen plateau (Southern Indian Ocean). In *Green Marine Clays* (ed. G. S. Odin), pp. 277–294. Elsevier, Amsterdam.
- Odin G. S., Bailey S. W., Amouric M., Frohlich F., and Waychunas G. A. (1988) Mineralogy of the facies verdine. In *Green Marine Clays* (ed. G. S. Odin), pp. 159–206. Elsevier, Amsterdam.
- Parfitt R. L. and Childs C. W. (1988) Estimation of forms of Fe and Al: A review, and analysis of contrasting soils by dissolution and Moebauer methods. *Aust. J. Soil Res.* **26**, 121–144.
- Porrenga D. H. (1967) Glauconite and chamosite as depth indicators in the marine environment. *Mar. Geol.* **5**, 495–501.
- Rabouille C., Galliard J.-F., Treguer P., and Vincendeau M.-A. (1997) Biogenic silica recycling in surficial sediments across the Polar Front of the Southern Ocean (Indian Sector). *Deep-Sea Res.* **44**, 1151.
- Ragueneau O., Tréguer P., Leynaert A., Anderson R. F., Brzezinski M. A., DeMaster D. J., Dugdale R. C., Dymond J., Fischer G., François R., Heinze C., Maier-Reimer E., Martin-Jézéquel V., Nelson D. M., and Quéguiner B. (2000) A review of the Si cycle in the modern ocean: Recent progress and missing gaps in the application of biogenic opal as a paleoproductivity proxy. *Global and Planetary Change* **26**, 317–365.
- Raiswell R., Whaler K., Dean S., Coleman M. L., and Briggs D. E. G. (1993) A simple three-dimensional model of diffusion-with-precipitation applied to localised pyrite formation in framboids, fossils and detrital iron minerals. *Mar. Geol.* **113**, 89–100.
- Rickert D., Schlüter M., and Wallmann K. (2002) Dissolution kinetics of biogenic silica from the water column to the sediments. *Geochim. Cosmochim. Acta* **66**, 439–455.
- Ristvet B. L. (1978) Reverse weathering reactions within recent nearshore marine sediments, Kaneohe Bay, Oahu. Test Directorate Field Command, Kirtland AFB, New Mexico.
- Robbins J., Heath G. R. and Lyle M. W. (1984) A sequential extraction procedure for partitioning elements among coexisting phases in marine sediments. Corvallis, Oregon State Univ., College of Oceanography Ref. 84-3, 55 pp.
- Rude P. D. and Aller R. C. (1994) Fluorine uptake by Amazon continental shelf sediments and its impact on the global fluorine cycle. *Cont. Shelf Res.* **14**, 883–907.
- Rude P. D. and Aller R. C. (1989) Early diagenetic alteration of lateritic particle coatings in Amazon continental shelf sediment. *J. Sed. Pet.* **59**, 704.
- Russell K. L. (1970) Geochemistry and halmrolysis of clay minerals, Rio Ameca, Mexico. *Geochim. Cosmochim. Acta* **34**, 893–907.
- Ryther J. H., Menzel D. W., and Corwin N. (1997) Influence of the Amazon River outflow on the ecology of the western tropical Atlantic. I. Hydrology and nutrient chemistry. *J. Mar. Res.* **25**, 69–82.
- Savin S. M. and Epstein S. (1970) The oxygen and hydrogen isotope geochemistry of clay minerals. *Geochim. Cosmochim. Acta* **34**, 43–63.

- Sayles F. L. (1979) The composition and diagenesis of interstitial solutions - I. Fluxes across the seawater-sediment interface in the Atlantic Ocean. *Geochim. Cosmochim. Acta* **43**, 527-545.
- Sayles F. L. and Bischoff. (1973) Ferromagnesian sediments in the equatorial east Pacific. *Earth Planet. Sci. Lett.* **19**, 330-336.
- Sayles F. L. and Mangelsdorf P. C. Jr. (1979) Cation-exchange characteristics of Amazon River suspended sediment and its reaction with seawater. *Geochim. Cosmochim. Acta* **43**, 767-780.
- Shiller A. M. (1996) The effect of recycling traps and upwelling on estuarine chemical flux estimates. *Geochim. Cosmochim. Acta* **60**, 3177-3185.
- Sholkovitz E. R. and Price N. B. (1980) The major-element chemistry of suspended matter in the Amazon Estuary. *Geochim. Cosmochim. Acta* **44**, 163-171.
- Showers W. J. and Angle D. G. (1986) Stable isotopic characterization of organic carbon accumulation on the Amazon continental shelf. *Cont. Shelf Res.* **6**, 227-244.
- Smith W. O. Jr. and DeMaster D. J. (1996) Phytoplankton biomass and productivity in the Amazon River plume: Correlation with seasonal river discharge. *Cont. Shelf Res.* **16**, 291-319.
- Sommerfield C. K., Nittrouer C. A., and Figueiredo A. G. (1995) Stratigraphic evidence of changes in Amazon shelf sedimentation during the late Holocene. *Mar. Geol.* **125**, 351-371.
- Strickland J. D. and Parsons T. R. (1968) A practical handbook of seawater analysis. *Fish. Res. Bd. Can. Bull.* **167**, 1-309.
- Tardy Y. (1997) *Petrology of Laterites and Tropical Soils*. A. A. Balkema, Rotterdam, 408 pp.
- Tréguer P., Nelson D. M., Van Bennekom A. J., DeMaster D. J., Leynaert A., and Queguiner B. (1995) The silica balance in the world ocean: A reestimate. *Science* **268**, 375-379.
- Turner R. E. and Rabalais N. N. (1994) Coastal eutrophication near the Mississippi river delta. *Nature* **368**, 619-621.
- Van Bennekom A. J. and Van Der Gast S. J. (1976) Possible clay structures in frustules of living diatoms. *Geochim. Cosmochim. Acta* **40**, 1149-1152.
- Van Bennekom A. J., Jansen J. H. F., Van Der Gast S. J., Van Iperen J. M., and Pieters J. (1989) Aluminium-rich opal: An intermediate in the preservation of biogenic silica in the Zaire (Congo) deep-sea fan. *Deep-Sea Res.* **36**, 173-190.
- Van Beusekom J. E. E., Van Bennekom A. J., Treguer P., and Morvan J. (1997) Aluminium and silicic acid in water and sediments of the Enderby and Crozet Basins. *Deep-Sea Res.* **44**, 987-1004.
- Van Cappellen P. and Qiu L. (1997a) Biogenic silica dissolution in sediments of the Southern Ocean. I. Solubility. *Deep-Sea Res.* **44**, 1109-1128.
- Van Cappellen P. and Qiu L. (1997b) Biogenic silica dissolution in sediments of the Southern Ocean. II. Kinetics. *Deep-Sea Res.* **44**, 1129-1150.
- Velde B. (1992) *Introduction to Clay Minerals*. Chapman & Hall, London, 198 pp.
- Wilkin R. T. and Barnes H. L. (1997) Formation processes of framboidal pyrite. *Geochim. Cosmochim. Acta* **61**, 323-339.
- Wollast R. (1974) The silica problem. In *The Sea*, Vol. 5 (ed. E. Goldberg), pp. 359-392. John Wiley, New York.
- Wollast R. and Mackenzie F. T. (1983) Global cycle of silica. In *Silicon Geochemistry and Biogeochemistry* (ed. S. R. Aston), pp. 39-76. Academic Press, New York.
- Yeh H.-W. and Eslinger E. V. (1986) Oxygen isotopes and the extent of diagenesis of clay minerals during sedimentation and burial in the sea. *Clays and Clay Minerals* **34**, 403-406.
- Zhu Z., Aller R. C., and Mak J. (2002) Stable carbon isotope cycling in mobile coastal muds of Amapá, Brazil. *Cont. Shelf Res.* **22**, 2065-2079.